1.0

1.1

1.25

4.5
5.0
5.6

2.8
3.2
3.6
4.0

2.5
2.2
2.0
1.8

1.4
1.6

MICROCOPY RESOLUTION TEST CHART
NATIONAL BUREAU OF STANDARDS 1963 A

AFWAL-TR-80-2041

LEVEL II

②

HIGH VOLTAGE SWITCH USING EXTERNALLY IONIZED PLASMAS

ADA086761

Westinghouse Electric Corporation
Systems Development Division
Baltimore, Maryland 21203

DTIC
SELECTED
JUL 16 1980
E

April 1980

TECHNICAL REPORT AFWAL-TR-80-2041

Final Report for Period 26 June 1978 – 21 December 1979

AERO PROPULSION LABORATORY
AIR FORCE WRIGHT AERONAUTICAL LABORATORIES
AIR FORCE SYSTEMS COMMAND
WRIGHT-PATTERSON AIR FORCE BASE, OHIO 45433

80 7 7 100

Project Engineer
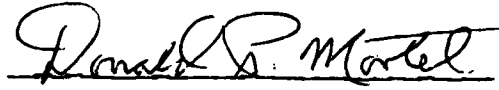Energy Conversion Branch

DONALD P. MORTEL
Actg Chief, Energy Conversion Branch
Aerospace Power Division

FOR THE COMMANDER

ROBERT R. BARTHELEMY
Actg Chief, Aerospace Power Division
Aero Propulsion Laboratory

AIR FORCE/56780/19 June 1980 — 120

REPORT DOCUMENTATION PAGE	READ INSTRUCTIONS BEFORE COMPLETING FORM

1. REPORT NUMBER	2. GOVT ACCESSION NO.	3. RECIPIENT'S CATALOG NUMBER
AFWAL-TR-80-2041	AD-A086 767	

4. TITLE (and Subtitle)	5. TYPE OF REPORT & PERIOD COVERED
High Voltage Switch Using Externally Ionized Plasmas	Final Technical Report June 26, 1978-Dec. 21, 1979
	6. PERFORMING ORG. REPORT NUMBER DYD-55585-AA

7. AUTHOR(s)	8. CONTRACT OR GRANT NUMBER(s)
John W. Dzimianski (ATL) Laurence E. Kline (Research Laboratories)	F33615-78-C-2010

9. PERFORMING ORGANIZATION NAME AND ADDRESS	10. PROGRAM ELEMENT, PROJECT, TASK AREA & WORK UNIT NUMBERS
Westinghouse Electric Corporation Systems Development Division Baltimore, Md 21203	2301 S2 05

11. CONTROLLING OFFICE NAME AND ADDRESS	12. REPORT DATE
Aero Propulsion Laboratory (AFWAL/POOC-3) Air Force Wright Aeronautical Laboratories Wright-Patterson AFB, Ohio 45433	April 1980
	13. NUMBER OF PAGES 80

14. MONITORING AGENCY NAME & ADDRESS(if different from Controlling Office)	15. SECURITY CLASS. (of this report)
Same	UNCLASSIFIED
	15a. DECLASSIFICATION/DOWNGRADING SCHEDULE N/A

16. DISTRIBUTION STATEMENT (of this Report)

Approved for public release; distribution unlimited.

17. DISTRIBUTION STATEMENT (of the abstract entered in Block 20, if different from Report)

18. SUPPLEMENTARY NOTES

Project Engineer: Dr. Peter Bletzinger (AFWAL/POOC-3)

19. KEY WORDS (Continue on reverse side if necessary and identify by block number)

e-beam, plasma, switch, high voltage, high current, thin-film field emission, electron transport data, breakdown, N_2, Ar, CH_4

20. ABSTRACT (Continue on reverse side if necessary and identify by block number)

A physical model was developed and the performance parameters were studied for high-voltage high-current on/off switches which use the low energy secondary electrons in an electron beam (e-beam) sustained discharge as the conducting medium. The model equations are presented and described along with the underlying physical assumptions. Electron transport data and static breakdown voltages were calculated for N_2, Ar, a N_2: Ar = 1:9 mixture

DD FORM 1473 EDITION OF 1 NOV 65 IS OBSOLETE

and CH_4^n by numerically solving the Boltzman equation to find the energy distribution. Study of steady state performance for N_2, Ar, N_2^n:Ar = 1:9 and CH_4^n indicated that the N_2^n:Ar = 1:9 and CH_4^n were both good candidate gases; hence transient switch performance were studied for these two gases. The performance of the e-beam plasma switches were mapped in a regime where the power delivered to the load is much greater than the e-beam power. Study of e-beam sources pointed to the thin-film field emission cathode as offering a means of controlling e-beam plasma switches with very high control power gain. A switch geometry was suggested using such an e-beam source. The comparison of different switch types with on/off capability indicated that the e-beam externally ionized plasma switches have the potential to be developed into devices that would be competitive or superior in size and capability with any other approach providing equivalent electrical performance.

TABLE OF CONTENTS

Accession For

NTIS GRA&I
DDC TAB
Unannounced
Justification

By

Distribution/

Availability Codes

Dist | Avail and/or
special

A

LIST OF ILLUSTRATIONS

LIST OF ILLUSTRATIONS (Continued)

LIST OF TABLES

SECTION I
INTRODUCTION AND SUMMARY

The objective of the "High Voltage Switch Using Externally Ionized Plasmas" study was to apply the theoretical methods developed for modeling high power gas lasers to study the feasibility and performance parameters of an externally ionized discharge used as a high-voltage, high-current switch with "on" and "off" capability. The principal emphasis of the effort was directed toward the analysis of the plasma-discharge parameters and the derivation of the equations for a computer program that modeled the operation of high-voltage on/off switches which use an electron-beam ionized-discharge plasma as the conducting medium. The computer program on punched cards and the Users Manual were delivered under separate cover. Other topics covered in the study included external ionization sources, gas/gas mixtures, switch geometry, and a comparison of different switch types with on/off capability.

Studied were the performance parameters for high-voltage on/off switches which use the low-energy secondary electrons in an electron-beam (e-beam) sustained discharge as the conducting medium. The discharge conductivity is negligible before the e-beam is turned on because the applied voltage is below the static breakdown voltage. When the e-beam is turned off, the discharge conductivity decays at a rate determined by the initial electron density and the electron recombination and attachment properties of the gas in the discharge volume.

The feasibility of such switches has been demonstrated experimentally.[1-3] However, most of these experiments studied a regime where both the e-beam current density, j_b, and the discharge current density, j, were high. Typically $j_b \sim 0.5$-5

A/cm^2 and j ∼ 25-500 A/cm^2. In this regime the e-beam power is comparable to the power delivered to the load because the current gain, j/j_b, is low and the e-beam voltage is 5-10 times the load voltage.

The performance of e-beam switches was mapped in a regime where the e-beam current density is j_b = 0.1-100 mA/cm^2. Since the current gain varies as $1/\sqrt{j_b}$, the power delivered to the load in this low e-beam current density regime is typically much greater than the e-beam power. In this regime, the switch efficiency, defined as the load power divided by the sum of the load, e-beam, and discharge powers, is limited by the power dissipated in the switch discharge. The feasibility of this regime has also been demonstrated experimentally.[2]

Electron transport data and static breakdown voltages are required to predict e-beam switch performance. These quantities were calculated for N_2, Ar, a N_2:Ar = 1:9 mixture, and CH_4 by numerically solving the Boltzmann equation to find the electron energy distribution. Both the N_2:Ar mixture and CH_4 have the desirable property that the electron drift velocity is high at low values of the electric field-to-gas density ratio, E/N. The predicted breakdown voltages are in good agreement with experiment.

Three steady-state switch properties were predicted for the gases and the mixture listed above: 1) current gain, 2) area required for total currents of 1 kA and 20 kA, and 3) efficiency, as defined above. Also predicted were turn-on and turn-off times for the N_2:Ar mixture and CH_4.

A study was made of what type of electron-beam source would be most advantageous for the switch application. Considered were thermionic, plasma cathode, ion plasma, field emission, and thin-film field emission electron sources. It was found that the thin-film field emission cathode runs at only 100 to 200 volts which is a voltage level compatible with power transistor circuitry and furthermore, offers a means of controlling the externally ionized plasma switch with a very high control power gain. This may be the

key factor for making this type of switch superior to any other competitive approach. The switch geometry suggested in this study incorporates a thin-film field emission cathode as the electron source. The comparison of different switch types with on/off capability indicated that the e-beam plasma switch has the potential of being developed into a device that would be competitive or superior in size and capability with any other appraoch providing equivalent electrical performance.

SECTION II
ELECTRON-BEAM PLASMA SWITCH STUDY

2.1 MODEL DESCRIPTION

This section describes the physical model that is used to predict the performance of electron-beam ionized plasmas as high-voltage on/off switches (e-beam switches). The model equations are presented and described along with the underlying physical assumptions. The plasma and circuit models are described first. Then we describe the model which is used to characterize the electron-beam source.

2.1.1 Plasma and Circuit Models

The plasma model used to predict the steady state and transient operation of the e-beam switch is based on the assumption that the plasma properties are spatially uniform throughout the discharge volume. Cathode- and anode-sheath regions are neglected. In the plasmas of interest, high conductivity is obtained as long as electrons are the dominant current carriers. In addition, the electrons play a crucial role in the breakdown of the gas. Hence, the electron drift velocity, mean energy, and attachment rate coefficient (for attaching gases) must all be known as a function of E/N, the electric field-to-gas density ratio, in order to predict switch performance. These quantities have been calculated for argon, nitrogen, a 10 percent nitrogen-90 percent argon mixture, and methane by numerically solving the Boltzmann equation to find the electron energy distribution. The method and computer code used are described in reference 4. Since the electron current is expected to be dominant in cases of interest, ionic currents are neglected in the transient calculations. This assumption can be checked by comparing the calculated electron density with the calculated ion density.

Negative ions are neglected completely in the steady-state cal-
culations. This assumption can be checked by comparing the
calculated transient and steady-state results for identical
conditions.

The three differential equations that describe the plasma
are:

$$\frac{dn_e}{dt} = S + (\alpha - a) \quad Wn_e - k_3N^2 \, n_e - k_r \, n_+ \, n_e \tag{1}$$

$$\frac{dn_+}{dt} = S + \alpha Wn_e - k_r \, n_e \, n_+ - k_i \, n_- \, n_+ \tag{2}$$

$$\frac{dn_-}{dt} = aWn_e + k_3N^2 \, n_e - k_i \, n_+ \, n_- \tag{3}$$

Where S is the electron beam electron-ion pair production
rate, α and a are the electron-impact ionization and dissociative
attachment rates, k_3 is a 3-body attachment rate, k_r is the elec-
tron-ion recombination rate, and k_i is the ion-ion recombination
rate. The symbols n_e, n_+, and n_- denote, respectively, the
electron, *positive ion and negative* ion densities. These
equations are integrated numerically in the transient calculation
along with a fourth differential equation for the power supply
circuit:

$$\frac{dV_c}{dt} = I/C \tag{4}$$

V_c is the power supply capacitor voltage and I is the current
in the circuit assumed which is shown in figure 1.

The plasma particle densities are related to the total
current by:

$$I = (n_e W + n_+ \, W_+ + n_- \, W_-) \, q_e \, A \tag{5}$$

where W, W_+, and W_- are, respectively, the electron, positive
ion and negative ion drift velocities, q_e is the electron charge,
and A is the switch cross-sectional area.

Analysis of the circuit of figure 1 gives:

$$I = (V_c - V_s)/R_L \tag{6}$$
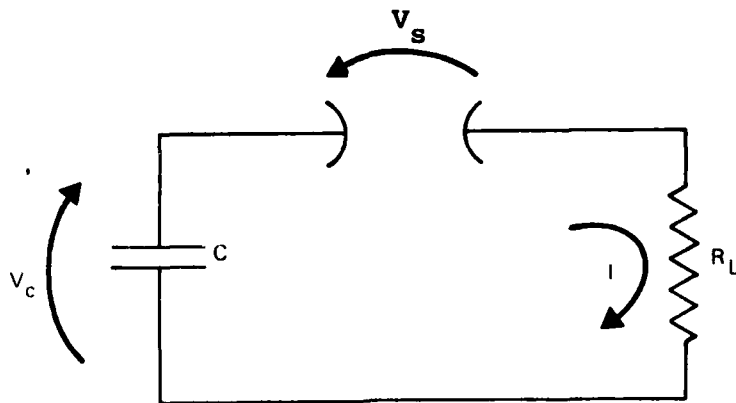
79-3151 VA 26

Figure 1.   Circuit Assumed in the Switch Computer Program

Equating equations (5) and (6) gives an expression for V_s:

$$V_s = \frac{V_c - C_1 (n_e a + n_+ a_+ + n_- a_-)}{1 + C_1 (n_e b + n_+ b_+ + n_- b_-)/Nd} \qquad (7)$$

where $C_1 = q_e A R_L$. R_L is the load resistance of figure 1. N is
the gas density, and d is the discharge gap length. The constants
a, b, a_+, a_- and b_- are fitting parameters for linearized approxi-
mations to the electron, positive-ion and negative-ion drift
velocities, denoted, respectively, as W, W_+, and W_-.

$$W \approx a + b \ (E/N)$$
$$W_+ \approx a_+ + b_+ \ (E/N)$$
$$W_- \approx a_- + b_- \ (E/N)$$

The linearization is done for each time step at the local E/N
value from the previous time step.

6

In the program as presently written, ionic conduction is neglected and equation (7) simplifies to:

$$V_s = \frac{V_c - C_1 n_e a}{1 + C_1 n_e / Nd} \tag{8}$$

Two additional differential equations are solved in the program. The first equation calculates the buildup of the density of dissociation products in the discharge due to electron-impact dissocation:

$$\frac{dN_d}{dt} = \alpha_d W n_e \tag{9}$$

where N_d is the time-dependent density of dissociation products in the discharge and α_d is the dissociation coefficient defined analogously to the ionization and attachment coefficients. The second equation calculates the temperature rise in the discharge volume due to the heat added by the discharge:

$$\frac{dT}{dt} = \frac{jE}{NC_p} \tag{10}$$

where j is the discharge current density and C_p is the specific heat of the gas or gas mixture. C_p has units of J/molecule $^\circ$K as defined in the program. T is the time-dependent gas temperature in $^\circ$K. N_d and T are not coupled with the other plasma properties in the present form of the model.

Steady-state plasma characteristics are calculated by solving equation (1) with $dn_e/dt = 0$. The resulting expression for n_{e_b}, the steady-state electron density, is:

$$n_{e_o} = \left(\nu_a - \sqrt{\nu_a^2 + 4k_r S} \right) / -2k_r \tag{11}$$

where $\nu_a = aW + k_3 N^2$ is the total electron loss rate due to attachment. The circuit assumed in the steady-state calculations is the same as the circuit of figure 1, except that a constant voltage power supply is assumed.

Experimentally, one would build a switch with a particular area, fill it with a gas (or gas mixture) and then test the

switch in a circuit to determine the switch voltage and current
as a function of gas fill, electron beam, and circuit parameters.
In the steady-state calculations, it is more convenient to
specify the ratio $R = V_s/V_p$ along with the values of the power
supply voltage, V_p, current I, and electron transport properties
of the assumed gas fill. Then the required switch area is
calculated as a function of the electron-beam parameters.

The values of E/N in the switch are determined by the
specified values of R, V_p and Nd. The value of Nd is chosen
so that the static switch breakdown voltage is $\approx 1.5 \times V_p$. When
n_{e_0} values have been calculated, the switch current density,
j, is determined from:

$$j = n_{e_0} q_e W(E/N) \tag{12}$$

The corresponding area required to carry the specified total
current is

$$A = I/j \tag{13}$$

The switch efficiency is defined as the power dissipated in the
load divided by the sum of the load, switch, and electron-beam
powers:

$$\eta = V_L I / (V_s I + V_b j_b A + V_L I) \tag{14}$$

where V_b and j_b are, respectively, the voltage and current
density of the electron-beam ionization source and $V_L = V_p - V_s$
is the load voltage.

2.1.2 Electron Beam Source Model

The ionization rate due to the electron beam is also assumed
to be spatially uniform in order to be consistent with the rest
of the plasma model.

The ionization rate, S, of equations (1) and (2) is given
by[5]:

$$S = \dot{J}_b N \left(\frac{Mm_p}{q_e E_i}\right) (dE/dm) \tag{15}$$

which can be rewritten as

$$S = \dot{J}_b N g \tag{16}$$

8

This expression is consistent with experimental results in nitrogen as discussed below and is widely used to predict the characteristics of electron-beam sustained laser discharges[6]. The definition of g in equation (16) follows from equation (15). The value of g is a function of the target gas (or gas mixture) and the electron-beam voltage. Values of g in equation (16) or dE/dm in equation (15) have been tabulated for many materials including gases relevant to e-beam switches. See, for example, references 5, 6, and 7.

2.2 GAS SELECTION: ELECTRON TRANSPORT AND DIELECTRIC PROPERTIES

The gas or gas-mixture properties required for externally ionized switches are quite diverse. In the conducting mode, a high conductivity is required. This requirement translates to a high electron-drift velocity. On the other hand, good dielectric strength is required while the switch is turned off. This requirement is best satisfied by gases with strong attachment reactions. However, attachment losses tend to greatly reduce the conductivity when the switch is conducting. Finally, fast turn-on and turn-off are required. The turn-on time is determined mainly by the source. However, the turn-off time depends on the recombination and attachment loss rates; i.e., on the gas properties.

In order to evaluate various candidate gases and gas mixtures, we have numerically solved the Boltzmann equation to find the electron-energy distribution. The results of these calculations include predicted values of the electron-drift velocity and mean energy, electron-impact ionization and attachment coefficients, and electron-ion recombination coefficients, all as a function of E/N. The gas breakdown voltages are also predicted as a function of the parameter gas density x gap length.

The gases studied were nitrogen, argon, a N_2:Ar = 1:9 mixture and methane. The suitability of each gas for use in an externally ionized switch is discussed in section 2.3. Nitrogen and argon were studied as representative molecular and atomic

gases. The N_2:Ar = 1:9 mixture was studied because 1) available experimental and theoretical data indicate that a mixture containing a small amount of a molecular gas in Ar, Kr or Xe has a high conductivity at low E/N, and 2) N_2:Ar mixtures are used in laser-triggered spark gaps where the required dielectric and plasma properties are similar to those needed in an e-beam switch. We studied methane (CH_4) because 1) it is representative of many hydrocarbon gases which have a high drift velocity at low values of E/N, and 2) because experimental data are available from externally ionized switch experiments which used CH_4 as the working gas. The electron transport properties of CH_4 have been studied at low E/N. However, we are not aware of any studies at the high E/N values which are required to predict breakdown voltages and switch operation during the transition from the "on" to the "off" condition. Therefore, we have performed a Boltzmann analysis for CH_4 covering the range 0.1 < E/N ≤ 500 Td.

A complete set of electron-impact cross-section data is required as input to the Boltzmann calculations. The cross sections used are as follows: In nitrogen we used the momentum transfer and vibrational cross sections of Engelhardt, Phelps, and Risk.[8] Their vibrational cross sections were increased by a factor of 1.5 for electron energies ϵ >1.7 eV as suggested by Levron and Phelps.[9] The nitrogen electronic cross sections of Cartwright et.al.[10] were used. The ionization cross section of Rapp and Englander-Golden,[11] increased by a factor of 1.15, gives good agreement between measured[12] and predicted ionization coefficients. In argon we used the momentum transfer cross section of Frost and Phelps,[13] and the ionization cross section of reference 8. The total excitation cross section of Schaper and Schiebner[14] was increased by a factor of 1.3 to give agreement between the predicted ionization coefficient and that measured by Kruithof.[15]

The CH_4 cross sections we used are as follows: The momentum transfer cross section of Duncan and Walker[16] was used in the electron energy range 0.01< ϵ < 4 eV. For energies greater than 4 eV the momentum transfer cross section was estimated by uniformly

reducing the total cross section measured by Brode[17] by a factor of 2/3. The vibrational cross section (for the ν_4 mode only) of Duncan and Walker[16] was used. There have been a number of studies of cross sections for VUV emission[18] as well as a measurement of the total dissociation cross section by Winters.[19] Most of these sections have qualitatively similar shapes. However, the VUV excitation cross sections are on the order of 10^{-19} cm^2, while the dissociation cross section has a peak value of 4×10^{-16} cm^2. We used the dissociation cross section of Winters[19] as a first estimate of the total electronic cross section. The remaining cross sections which we included are the attachment cross section of Sharp and Dowell[20] and the ionization cross section of Rapp and Englander-Golden.[21]

2.2.1 <u>Predicted Transport Coefficients and Paschen Curves</u>

The literature cross section sets for argon and nitrogen described above were used to calculated transport coefficient values for an $Ar:N_2 = 1.9$ mixture. Mixtures of a rare gas with a small admixture of a molecular gas are attractive for use in an externally ionized switch because such mixtures can have an electron-drift velocity significantly higher than the drift velocity of either constituent as pointed out by Long, Bailey, and Garscadden.[22] Our results for the $Ar:N_2 = 1:9$ mixture are given in figure 2. The calculated drift velocity values differ slightly from those of reference 22 because we use a 50 percent larger value for the nitrogen vibrational peak near 2eV, as discussed above.

The predicted values of the electron drift velocity, W, and mean energy, $\overline{\epsilon}$ were fitted to expressions of the form:

$$W = A \ (E/N)^B \quad \ldots\ldots\ldots\ldots\ldots\ldots\ldots\ldots\ldots\ldots\ldots (17)$$
$$\overline{\epsilon} = C \ (E/N)^D \quad \ldots\ldots\ldots\ldots\ldots\ldots\ldots\ldots\ldots\ldots\ldots (18)$$

in the range of E/N relevant to switch operation for each gas. The resulting values of A, B, C, and D are given in table 1 for N_2, Ar and the N_2:Ar mixture.

We calculated electron-ion recombination coefficients for N_2, Ar, and the N_2:Ar $= 1:9$ mixture by assuming an electron temperature,

11
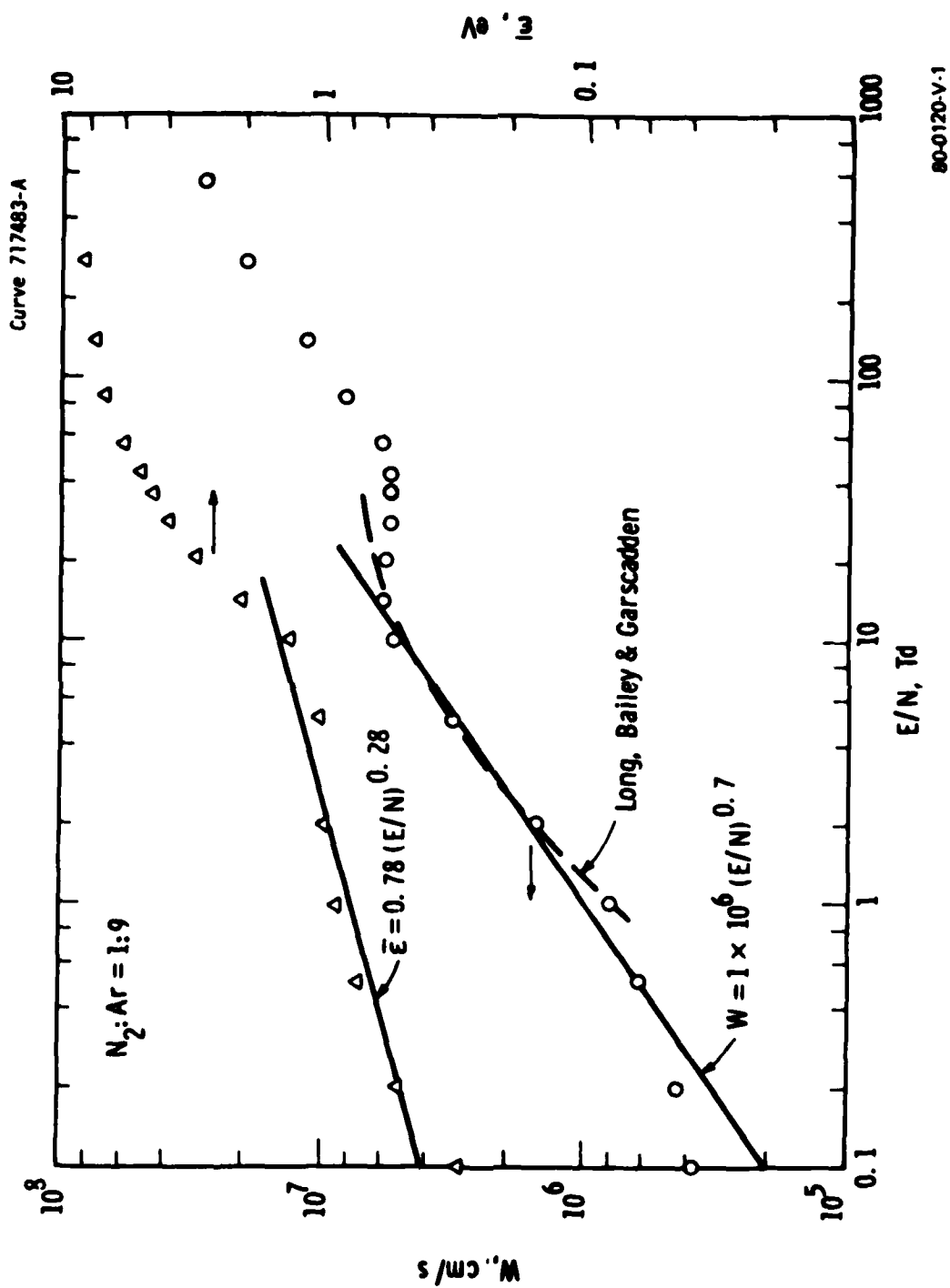
Figure 2. Calculated Electron Mean Energy and Drift Velocity for a N_2:Ar = 1:9 Mixture

12

TABLE 1

FITTING PARAMETERS USED TO EVALUATE THE ELECTRON DRIFT VELOCITY AND MEAN ENERGY IN THE NUMERICAL CALCULATIONS OF SWITCH CHARACTERISTICS

Gas	A	B	C	D	E	F	E/N Range, Td
Nitrogen	4×10^5	0.70	0.35	0.38	7.6×10^{-7}	-0.77	1 - 100
Argon	3.3×10^5	0.38	2.4	0.37	7.5×10^{-8}	-0.23	0.1 - 10
N_2:Ar = 1:9	1×10^6	0.70	0.78	0.28	1.6×10^{-7}	-0.17	0.2 - 20
Methane	3.8×10^6	0.60			2.4×10^{-7}	-0.34	0.2 - 10

80-0120-V-2

T_e, given by $kT_e/q_e = (2/3)\bar{\epsilon}$ where k is Boltzmann's constant and q_e is the electronic charge. The values of recombination rate coefficient vs. T_e of Douglas-Hamilton[23] in nitrogen, and Shiu and Biondi[24] in argon, were used in the calculations. In the N_2:Ar = 1:9 mixture we used the argon recombination rate coefficient because most of the primary ions will be Ar^+. This assumption is valid as long as rapid charge transfer reactions or assoication reactions do not compete with Ar_2^+ formation. The recombination rate coefficient values were fitted with functions of the form:

$$k_r = E \, \bar{\epsilon} \, F' \qquad (19)$$

or, substituting from equation (18):

$$k_r = E \, (E/N)^F \qquad (20)$$

The resulting values of E and F are given in table 1 for N_2, Ar, and the N_2:Ar = 1:9 mixture. Table 1 also gives values of A, B, E and F for methane based on the results described below.

We used the values $g = 32$ for nitrogen 23 and $g = 44$ for argon[24] and the $Ar:N_2 = 1.9$ mixture. These values of g correspond to an electron-beam voltage $V_b = 100$ kV.

Paschen curves, i.e., curves of the breakdown voltage V_s as a function of the gas density gap-length product at breakdown, Nd_s, have been measured for many common gases. However, Paschen curves are not available for many of the gas mixtures which are of possible interest for use in an externally ionized switch. Hence, a theoretical method of estimating Paschen curves is desirable. We have estimated Paschen curves using the expression:

$$[\alpha/N(E/N) - \eta/N (E/N)] Nd = k \qquad (21)$$

where α is the first Townsend ionization coefficient, η is the attachment coefficient and k is a constant. α/N and η/N are functions of E/N only. Hence, for any value of E/N, equation (21) can be solved to find the value Nd_s for which breakdown will occur. The corresponding breakdown voltage is given by:

$$V_s = (E/N) Nd_s \dots\dots\dots\dots\dots\dots\dots\dots\dots\dots\dots\dots\dots \qquad (22)$$

Equations (21) and (22) can be derived from the point-of-view of either the Townsend or streamer theories of breakdown.[25]

We have used Equations 21 and 22 to predict Paschen curves for argon, nitrogen, and an $Ar:N = 1:9$ mixture with the results shown in figure 3. We used the value $k = \ln (1 \times 10^8) = 18.4$ in all cases. We calculated α/N as a function of E/N by numerically solving the Boltzmann equation as discussed above. There is no attachment in these three gases. The predicted Paschen curve for nitrogen is in very good agreement with the experimental values collected by Dakin and Gerhold[26] as shown in figure 3. The agreement is not as good for argon, with the predicted V_s values lying 25 - 30 percent above measured values of Golden and Fischer.[27] The predicted Paschen curve for the $N_2:Ar = 0.1:0.9$ mixture is in good agreement with the experimental results of Guenther and Bettis.[28]

14

The results shown in figure 3 suggest that equations 21 and 22 are capable of predicting Pashchen curves for pure gases and gas mixtures. Therefore, a Paschen curve can be obtained for any specified gas mixture by solving the Boltzmann equation. The required input data is a set of electron collision cross sections for each component of the gas mixture. This approach has also been applied to SF_6:He and SF_6:N_2 mixtures with similar good agreement between theory and experiments.[29] The Paschen curves shown in figure 3 were used to select the Nd values in the numerical mapping of switch operating characteristics for N_2, Ar, and N_2:Ar=1:9 mixture which is described below.

Our results for methane are shown in figure 4, 5, and 6. For $0.1 < E/N < 20$ Td, the range studied by Duncan and Walker,[16] electronic excitation, ionization and attachment are unimportant. Duncan and Walker adjusted their momentum transfer and vibrational cross sections to give good agreement between measured and predicted values of the electron-drift velocity, W, and diffusion coefficient divided by mobility, D/μ, as shown in figure 4.

For $E/N > 20$ Td, electronic excitation and ionization become important. However, the predicted values of W and D are rather insensitive to changes in the magnitude of the electronic cross section, and predicted values of W and D/μ shown in figure 2 agree well with experiment [30-34] for E/N values up to ~ 250 Td. The predicted value of the net ionization coefficient, $(\alpha - a)/N$, are quite sensitive to the magnitude of the electronic cross section as shown in figure 5. When the total electronic cross section is taken to be 2.35 times the dissociation cross section the predicted net ionization coefficient values agree with the values measured by Cookson et al.[35] to within a factor of two or better over the range $70 < E/N < 500$ Td. Therefore we have used this value of the electronic cross section to predict the electron transport properties of CH_4.

We calculated the electron-ion recombination rate coefficient for methane by using the measured recombination cross-section of
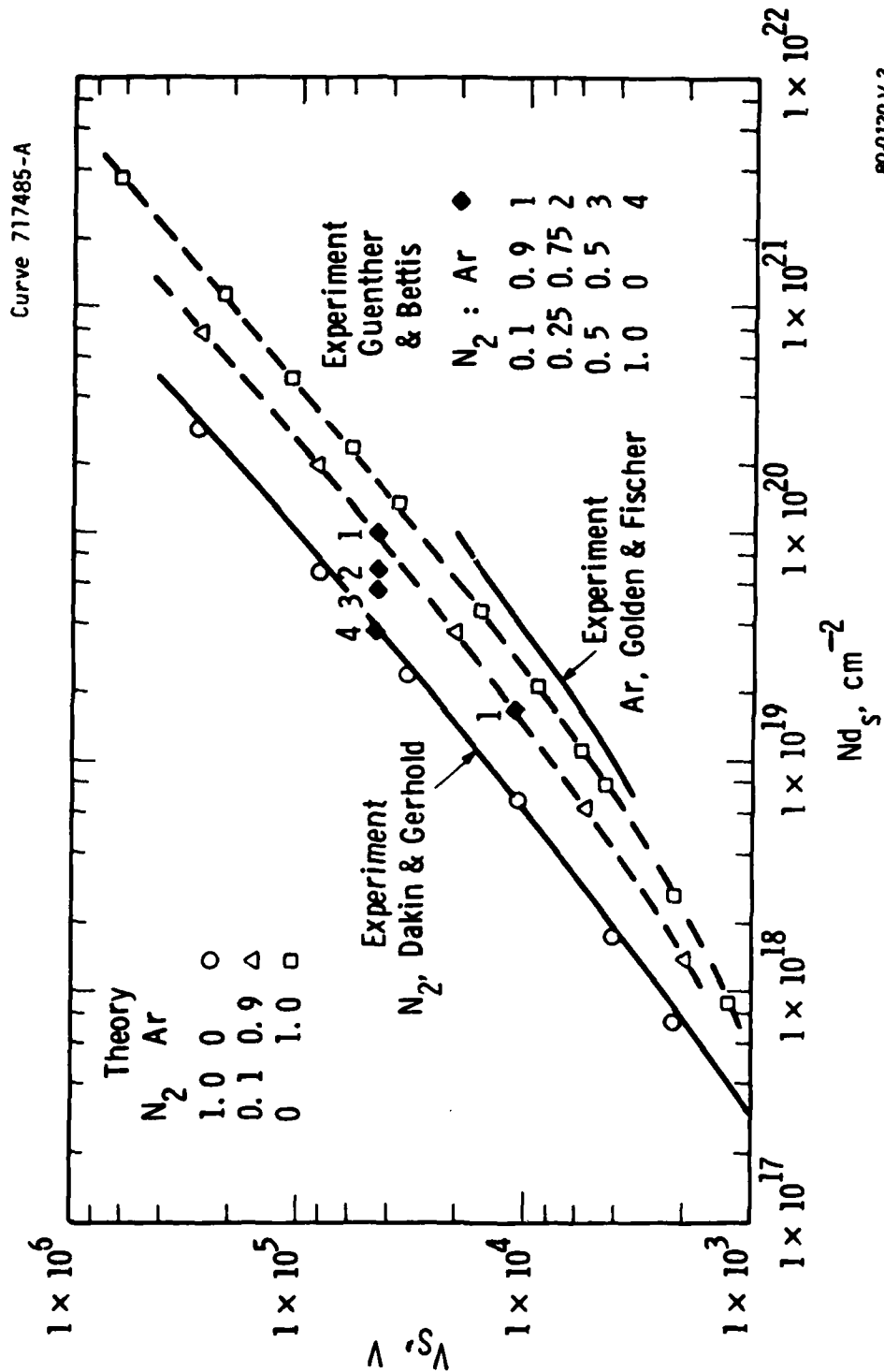
Figure 3. Calculated Paschen Curves for N_2, Ar, and a N_2:Ar 1:9 Mixture Compared with Experimental Paschen Curves
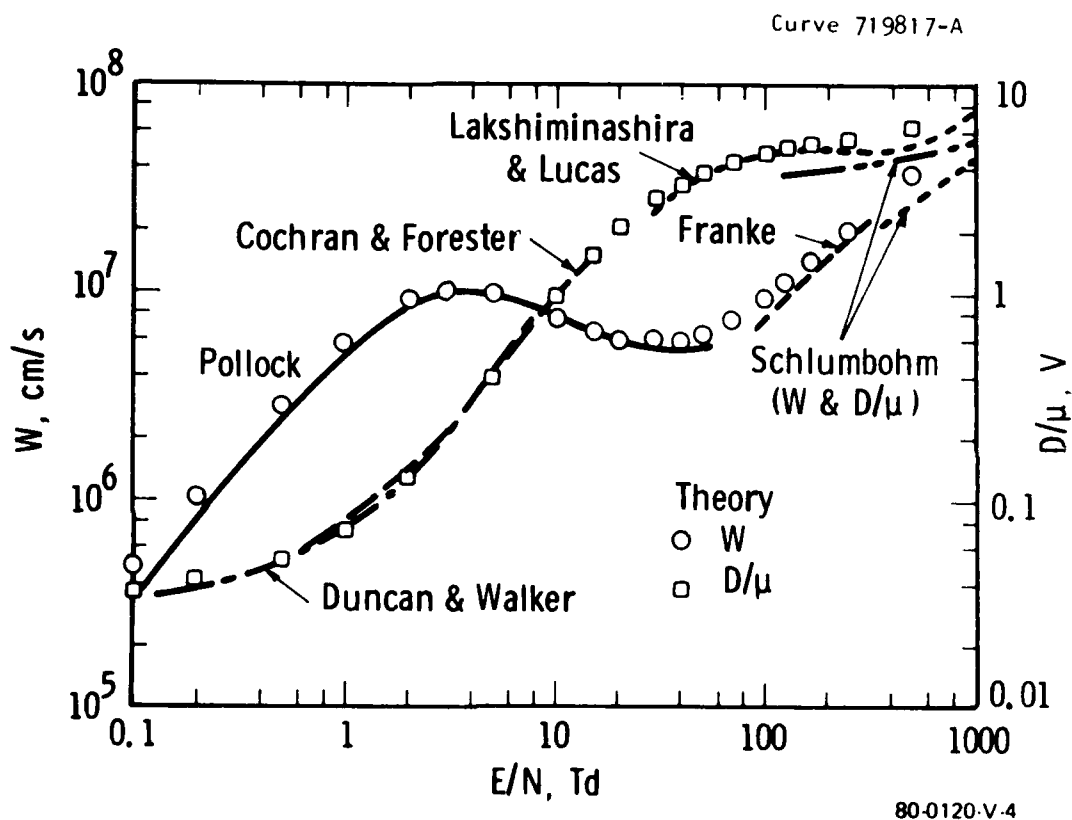
Figure 4. Measured and Predicted Electron Drift
Velocity and Diffusion Coefficient Over Mobility for Methane
(The experimental measurements are from references 16 and 30-34)

17
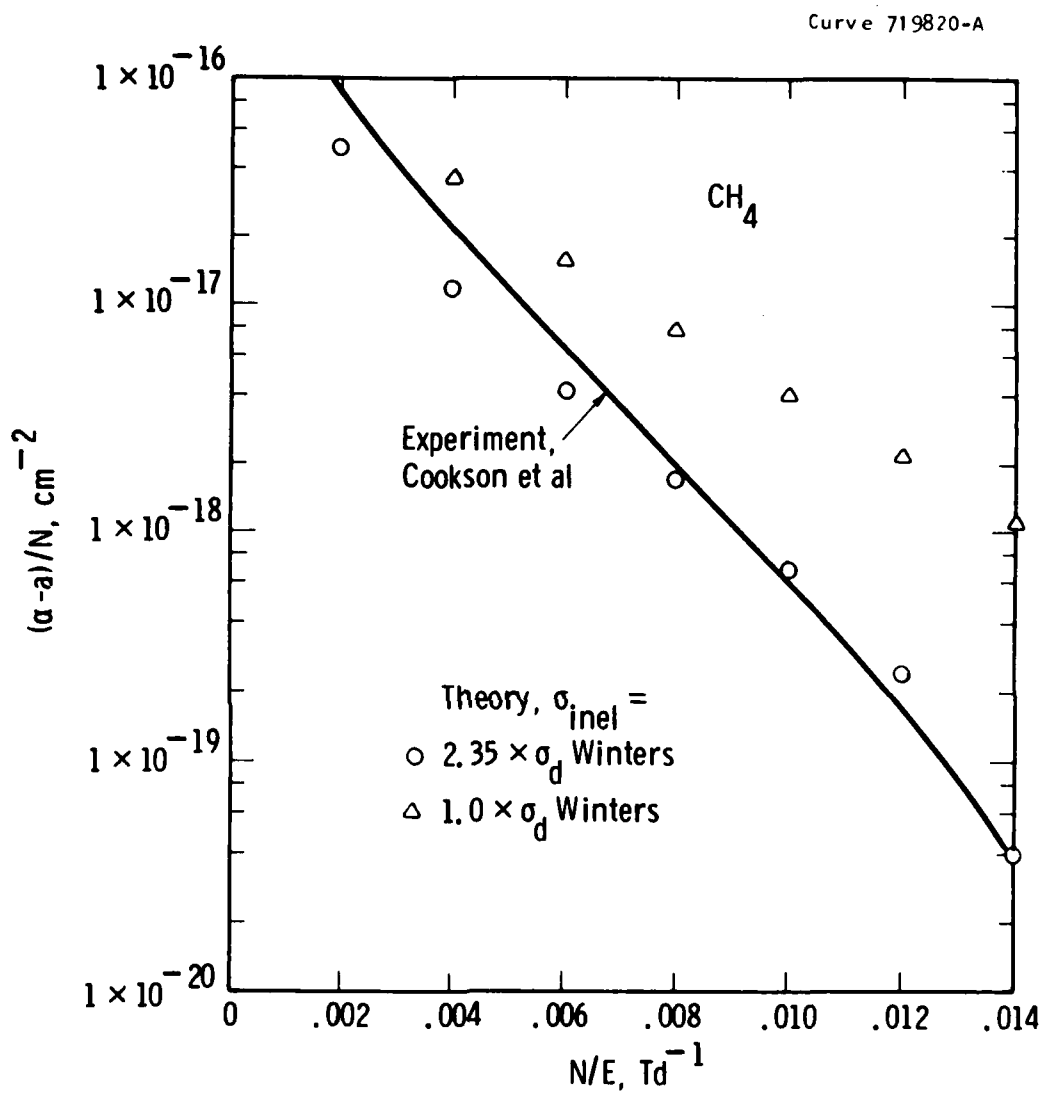
Figure 5. Measured and Predicted Net Ionization Coefficient for Methane

18

McGowan.[36] The calculated recombination rate is shown vs E/N in figure 6.

The values of g for methane were calculated from the dE/dm values given by Pages et.al,.[7] The resulting values are g = 28.6 for an e-beam voltage of 100 keV and g = 17.5 for an e-beam voltage of 250 keV.

In figure 7, we compare the Paschen curve predicted using equations 21 and 22 and the cross sections described above with various experimental measurements. The predicted breakdown voltages agree quite well with the experimental measurements of Cookson et. al.[25] Tholl[37] and Heylen and Lewis[38] with differences of 10 percent over a wide range of values of the scaling parameter Nd_s. The Paschen curve in figure 7 is used below to choose the values of Nd used in calculating switch operating characteristics for methane.

Curve 720520-A
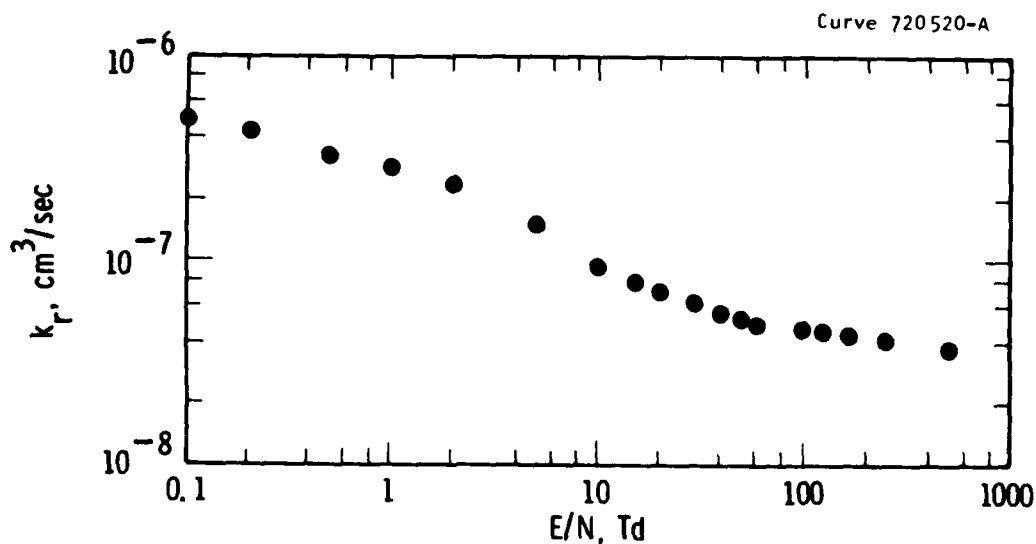
80-0120-V-6

Figure 6. Calculated Recombination Rate Coefficient Values for Methane
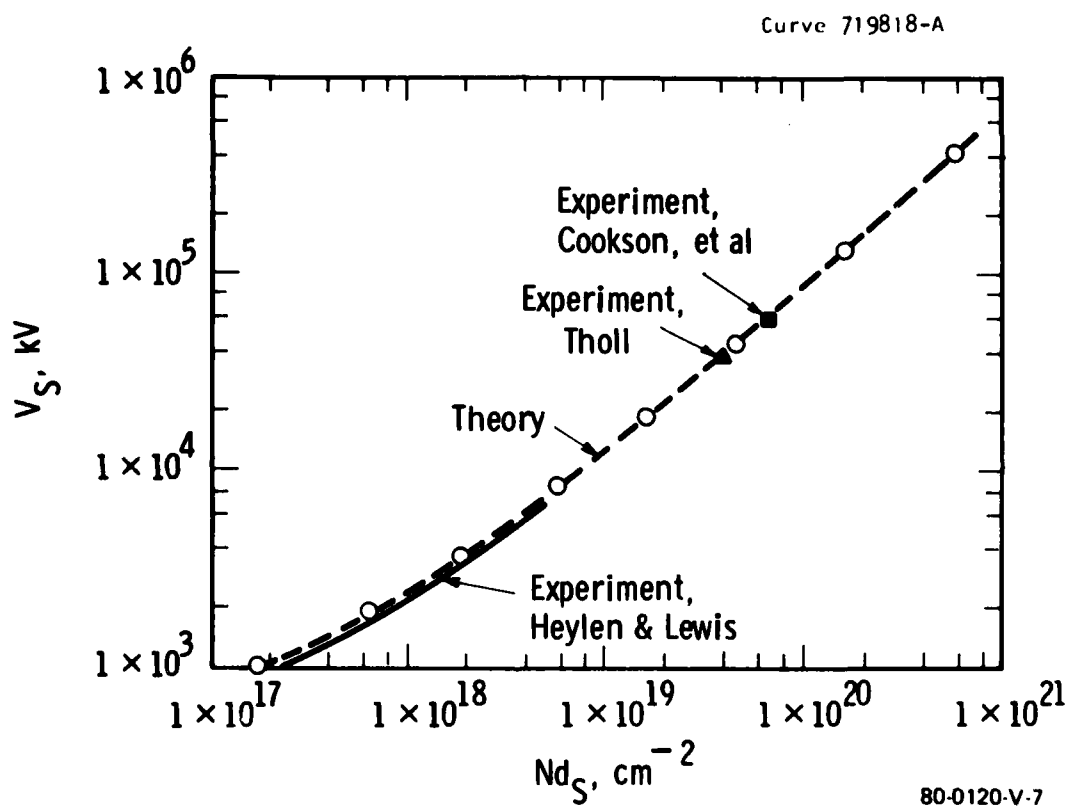
Figure 7. Measured and Predicted Paschen Curves for Methane

20

2.3 PARAMETER MAP/DESIGN GUIDE

This section describes the results of our steady state and transient performance calculations for electron-beam ionized, high-voltage on/off switches. Steady-state performance was studied for N_2, Ar, N_2:Ar = 1:9, and CH_4. The results of these steady-state calculations indicated that the N_2:Ar = 1:9 mixture and methane were both good candidate gases. Hence, we studied transient switch performance for these two gases.

2.3.1 Steady-State Switch Characteristics

We studied two switch operating regimes which are based on the switch performance guidelines suggested in the technical requirements section of this contract. The characteristics of the two operating regimes that we studied are listed in table 2.

The model outlined in equations (12) through (14) in section 2.1 was used to predict the steady-state switch characteristics

TABLE 2

SWITCH OPERATING REGIMES STUDIED

	Regime 1	Regime 2
Breakdown Voltage Across the Switch	150 kV	50 kV
Voltage at Which the Switch Can Turn Off	100 kV	33 kV
On Current	1 kA	20 kA
Switching Time (On or Off)	1-10 μs	1-10 μs
On Time*	10-500 μs	10-500 μs
Repetition Rate*	0-1 kHz	0-1 kHz
Current Gain	$\geq$ 1000	$\geq$ 1000
Lifetime	$\geq 10^6$ shots	$\geq 10^6$ shots

*High repetition rate coincides with short on time and long on time with low repetition rate.
 Also maximum number of pulses for any one event is 1000.

80-0120-V-8

21

for N_2, Ar, and the N_2:Ar=1:9 mixture, we used the electron-drift velocity, mean-energy values and the recombination rate coefficient values given by the curve fits of table 1. The remaining input data is described in section 2.2.

The values of the gas density and discharge gap length that we used in each case are listed in table 3. As discussed above, these values are based on our predicted breakdown curves. The Nd values given for methane are about twice the values required by breakdown considerations.

Steady-state characteristics have been determined for eight cases which are described in table 3. The results for nitrogen are given in figures 8, 9, and 10. The independent variables in figures 8-19 are the e-beam current density and the ratio of the switch voltage to the load voltage. The current gain, shown in figure 8, is high when the electron-beam current is small and the switch voltage is large. The same j/j_b curves apply to both the V_p = 100 kV, I = 1 kA case and the V_p = 33.3 kV, I = 20 kA case because the V_p, N, and d values have been chosen so that the E/N vs. V_s/V_L values are the same

TABLE 3

GAS AND CIRCUIT PARAMETER VALUES FOR THE CALCULATIONS
OF STEADY-STATE SWITCH CHARACTERISTICS

Gas	N, cm^{-3}	d, cm	V_p, kV	I, kA
Nitrogen	8.07×10^{19}	2	100	1
	8.07×10^{19}	0.667	33.3	20
Argon	1.35×10^{20}	6	100	1
	1.35×10^{20}	2	33.3	20
N_2:Ar = 1:9	8.1×10^{19}	5	100	1
	8.1×10^{19}	1.667	33.3	20
CH_4	1.08×10^{20}	4	100	1
	1.08×10^{20}	1.333	33.3	20

in each case. The values of switch area required for currents of 1 kA and 20 kA are shown in figure 9. The required area decreases as both the switch voltage and the electron-beam current increase. The values of the switch efficiency are given in figure 10 for both cases studied in nitrogen. The power required to drive the electron beam is unimportant except at small values of switch voltage (and power) and larger values of electron-beam current.

Results for argon are shown in figures 11, 12, and 13. Much larger Nd values are required in argon, compared with the Nd values for nitrogen, as shown in table 3. As a result the E/N values in argon are a factor of five smaller for any specified value of V_s. In addition, the drift velocity vs. E/N curve for argon lies below the drift velocity vs. E/N curve for nitrogen. These disadvantages are partially offset, at low E/N values by the much lower recombination rate in argon compared with nitrogen. However, over most of the parameter range studied, the current gain is lower and the required switch area is larger in argon compared with the corresponding results in nitrogen.

The results obtained in both nitrogen and argon indicate that a high electron-drift velocity, low electron loss rates and a high dielectric strength are the desired gas properties for an externally ionized switch. As discussed above, argon mixed with a small amount of nitrogen has an attractively high drift velocity, a dielectric strength approaching the strength of nitrogen, and a low recombination rate coefficient. We studied an $Ar:N_2 = 1:9$ mixture with the results shown in figures 14, 15, and 16. As expected, this mixture gives switch performance which is better than the performance obtained in either argon or nitrogen.

The results of the calaculations for methane are presented in figures 17, 18, and 19. Contours of constant current gain are plotted vs. beam current and switch voltage divided by load voltage in figure 17. Note that a current gain exceeding 1000 is obtained over a large part of the parameter space studied.

23

Curve 717481-A
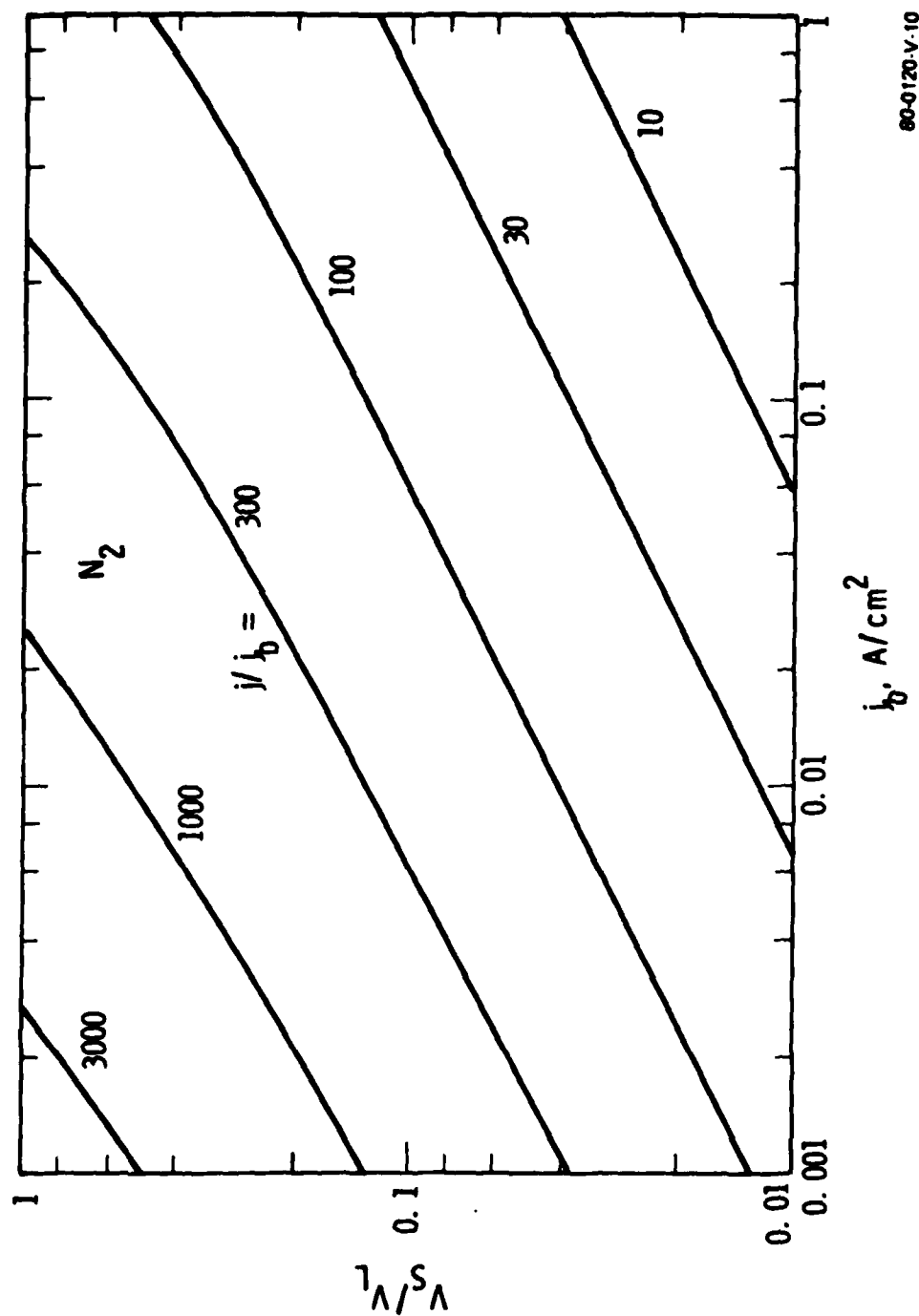
Figure 8. Switch Current Gain in Nitrogen. These Curves Apply to Both the V_p=100kV, I=1kA Case and the V_p=33.3kV, I=20kA Case

80-0120-V-10

24

Curve 717482-A

N_2

10 (200)

30 (600)

$A = 100 \text{ cm}^2$ (2000)

300 (6000)

1000 (20000)

3000 (60000)

10000 (200000)

V_S/V_L

1

0.1

0.01

0.001 0.01 0.1 1

j_b, A/cm^2

80-0120-V-11

Figure 9. Switch Areas in Nitrogen. The Area Required for a Current of 1kA is Given by the Values Next to the Curves. The Values in parenthesis are the Areas Required for a Current of 20 kA.

25
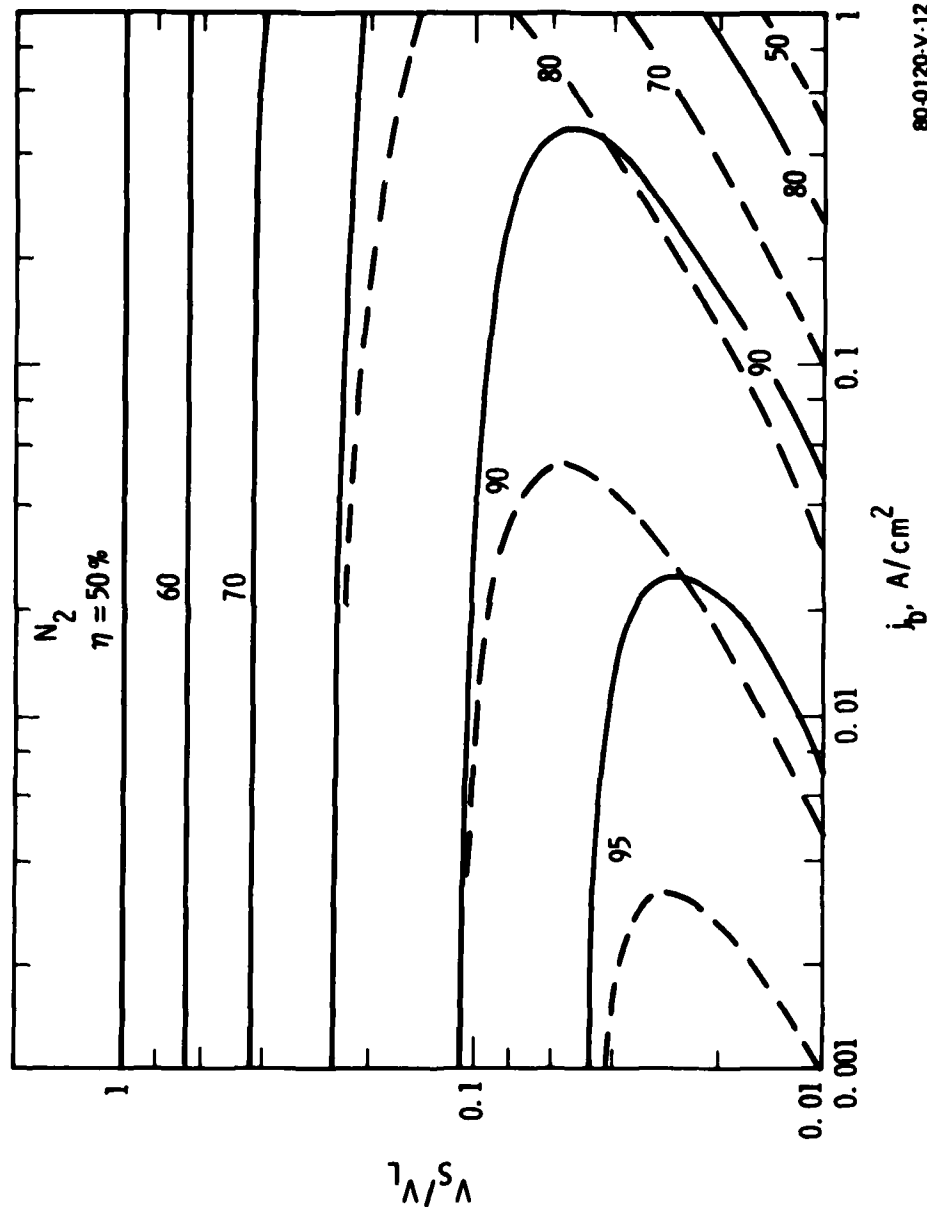
Curve 717480-A

Figure 10. Switch Efficiency in Nitrogen. The Solid Curves are for the V_p=100kV, I=1kA Case. The Dashed Curves are for the V_p=33.3kV, I=20kA Case.
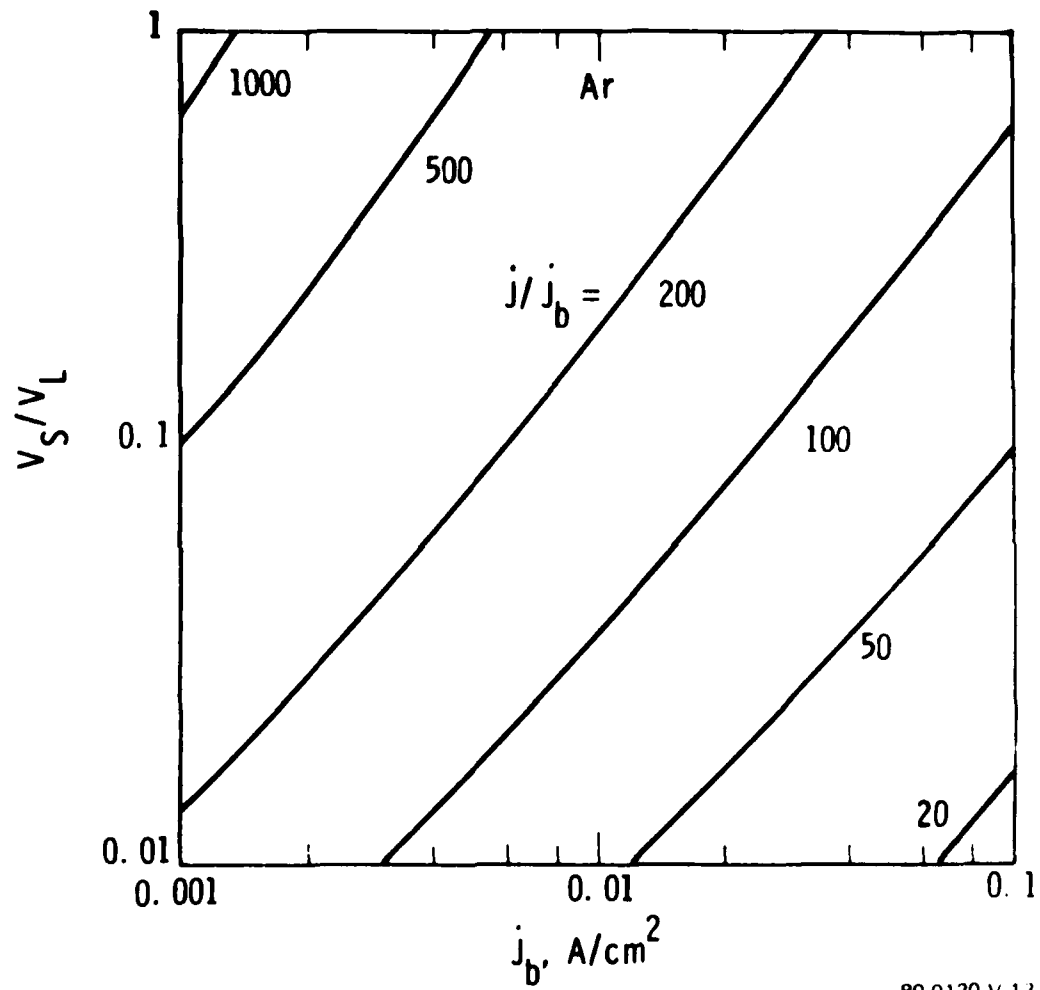
80-0120-V-12

Figure 11.   Switch Current Gain in Argon
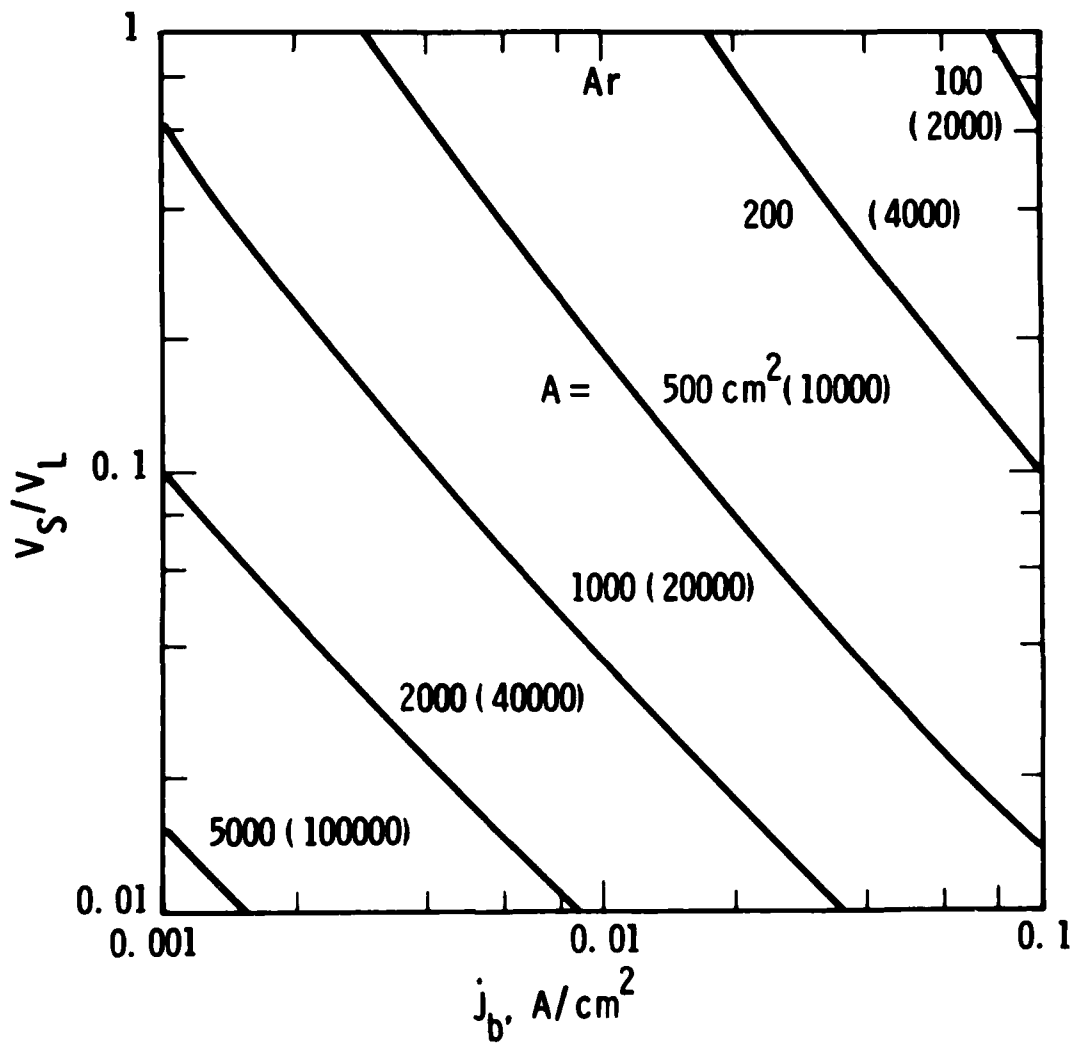
Figure 12. Switch Areas in Argon. The Area Required for a Current of 1kA is Given by the Values Next to the Curves. The Values in Parenthesis are the Areas Required for a Current of 20kA.

28
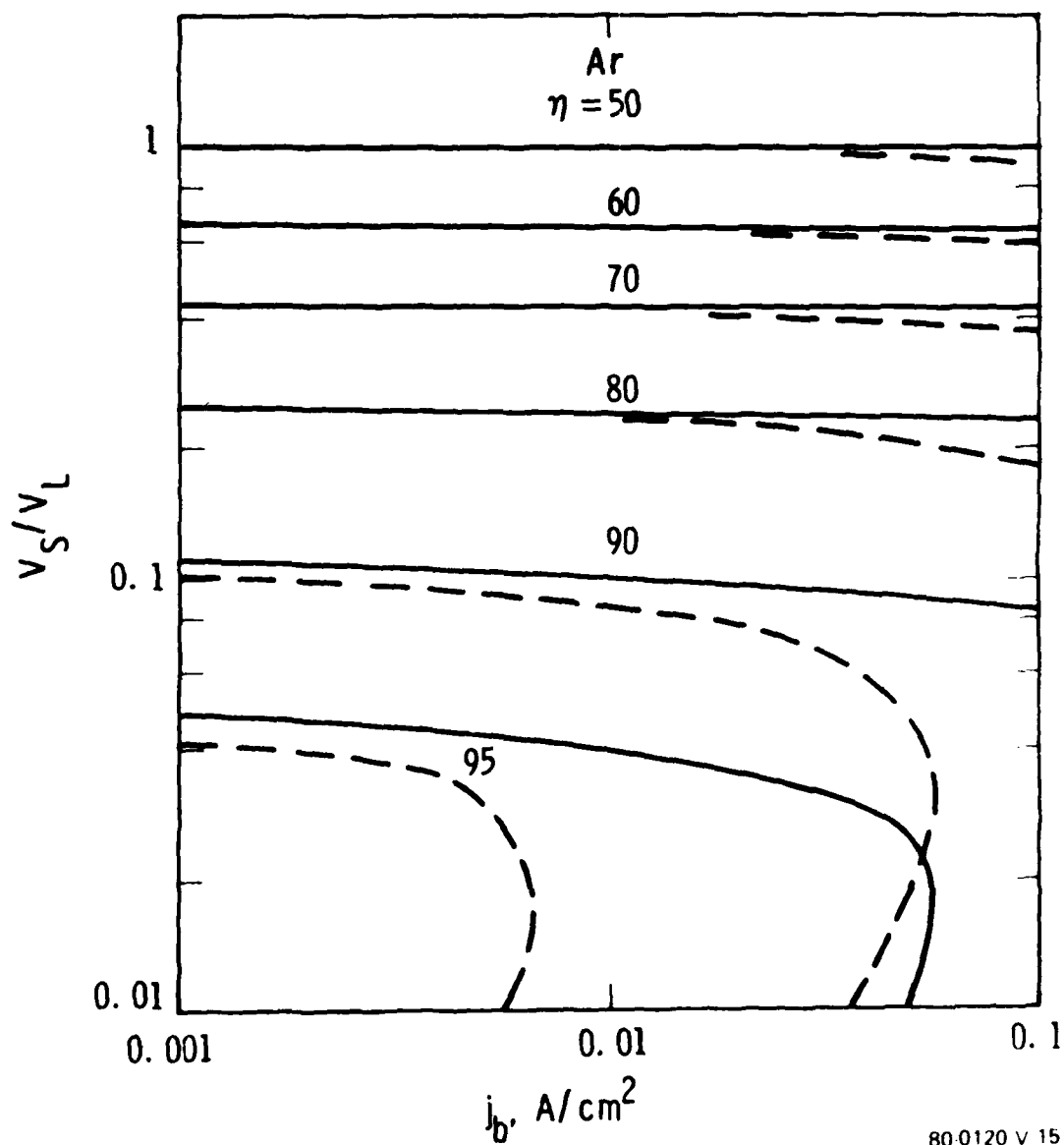
Figure 13. Switch Efficiencies in Argon. The Solid Curves are for the $V_p=100kV$, $I=1kA$ Case. The Dashed Curves are for the $V_p=33.3kV$, $I=20kA$ Case.

80·0120 V 15

Curve 717487-A

$N_2:Ar = 1:9$

$j/j_b =$

Figure 14. Switch Current Gain in a $N_2:Ar=1:9$ Mixture

80-0120-V-16

Curve 717486-A

N$_2$:Ar = 1:9

Area = 100 cm^2 (2000)

10 (200)
30 (600)
300 (6000)
1000 (20000)
3000 (60000)
10000 (200000)

j$_b$, A/cm^2

V$_S$/V$_L$
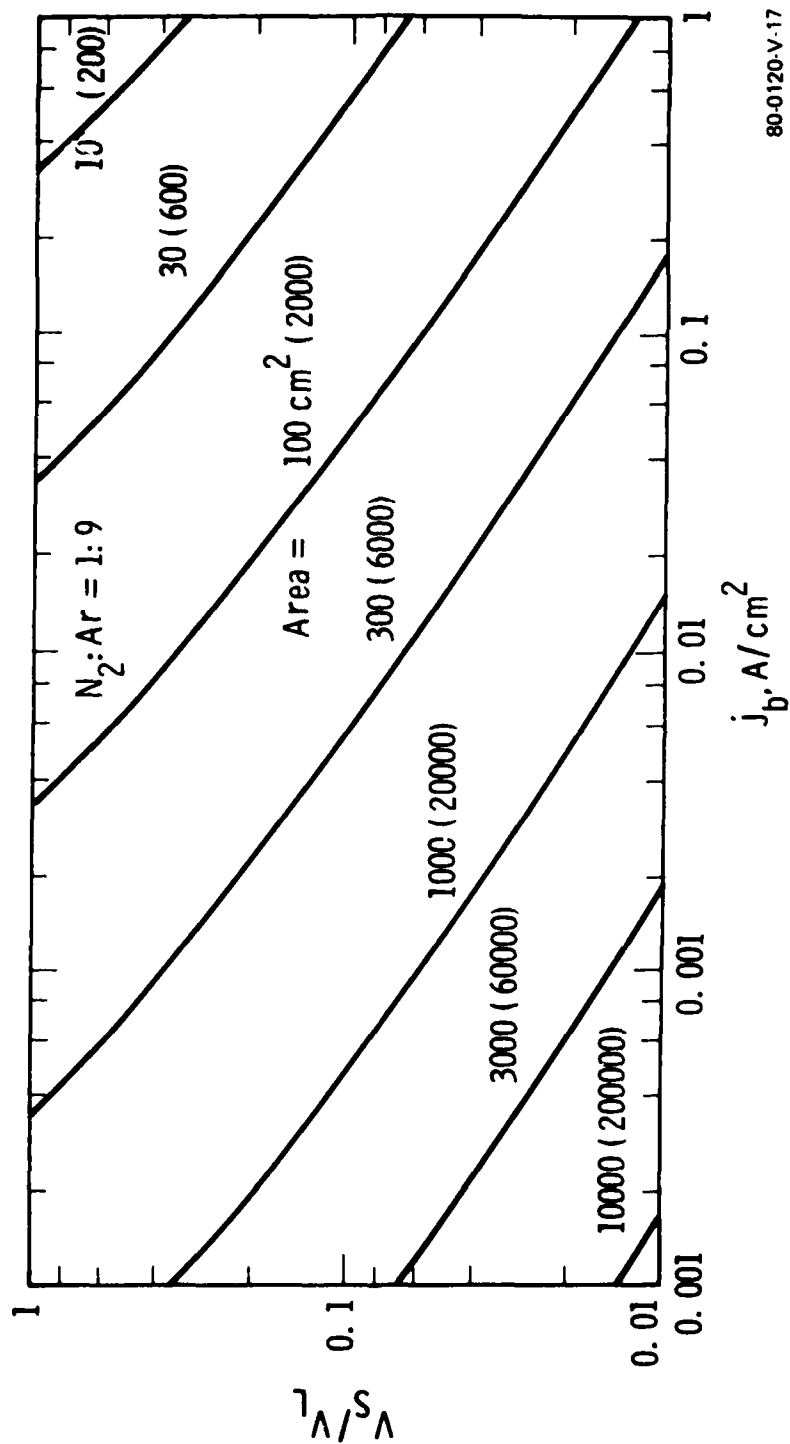
80-0120-V-17

Figure 15. Switch Areas in a N$_2$:Ar=1:9 Mixture. The Area Required for a Current of 1kA is Given by the Values Next to the Curves. The Values are in Parethesis are the Areas Required for a Current of 20kA.

31
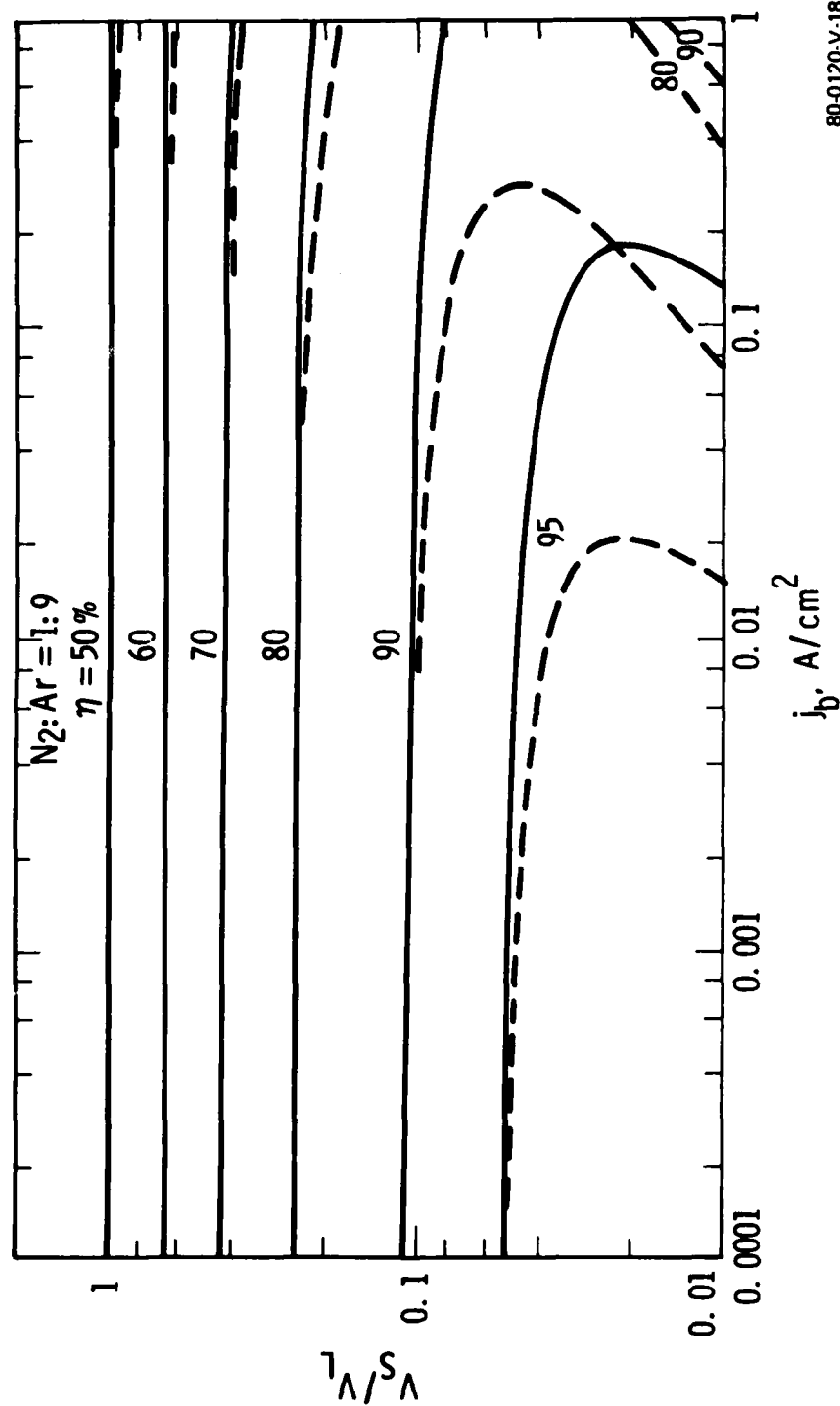
Figure 16. Switch Efficiency in a N₂:Ar=1:9 Mixture. The Solid Curves are for the Vp=100kV, I=1kA Case. The Dashed Curves are the for Vp=33.3kV, I≡20kA Case.

32
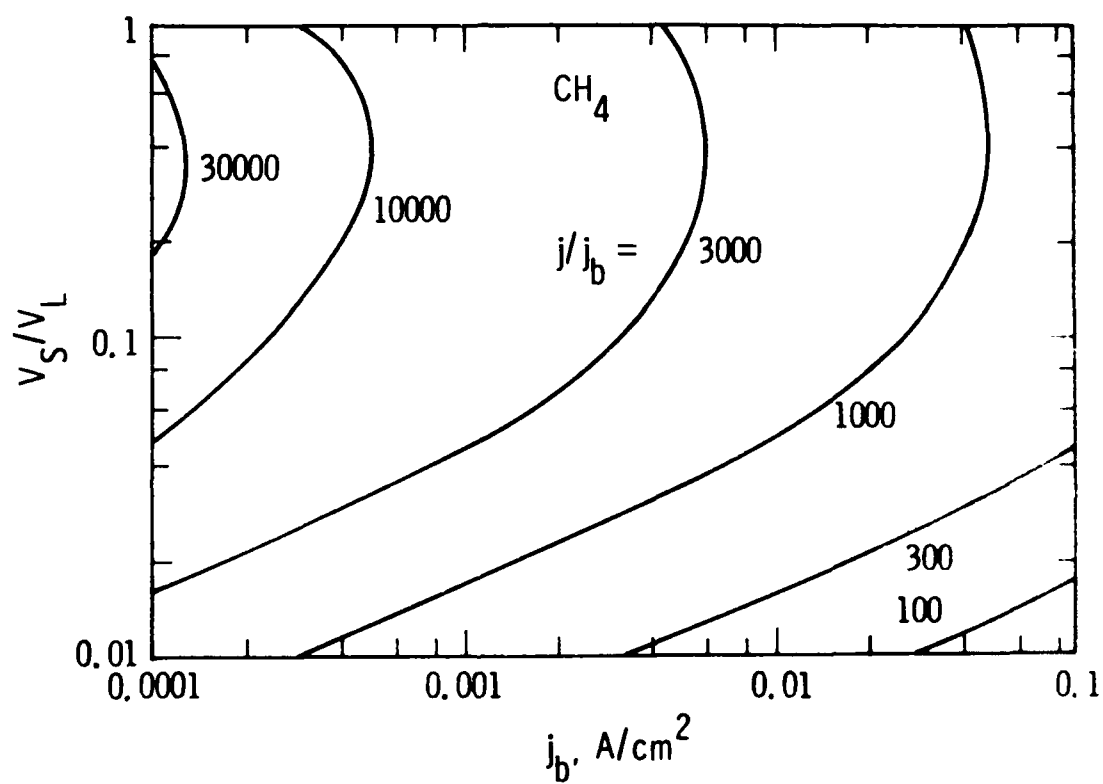
Figure 17. Switch Current Gain in Methane. These Curves Apply to Both the V_p=100kV, I≈1kA, and the V_p=33kV, I=20kA Case.

33
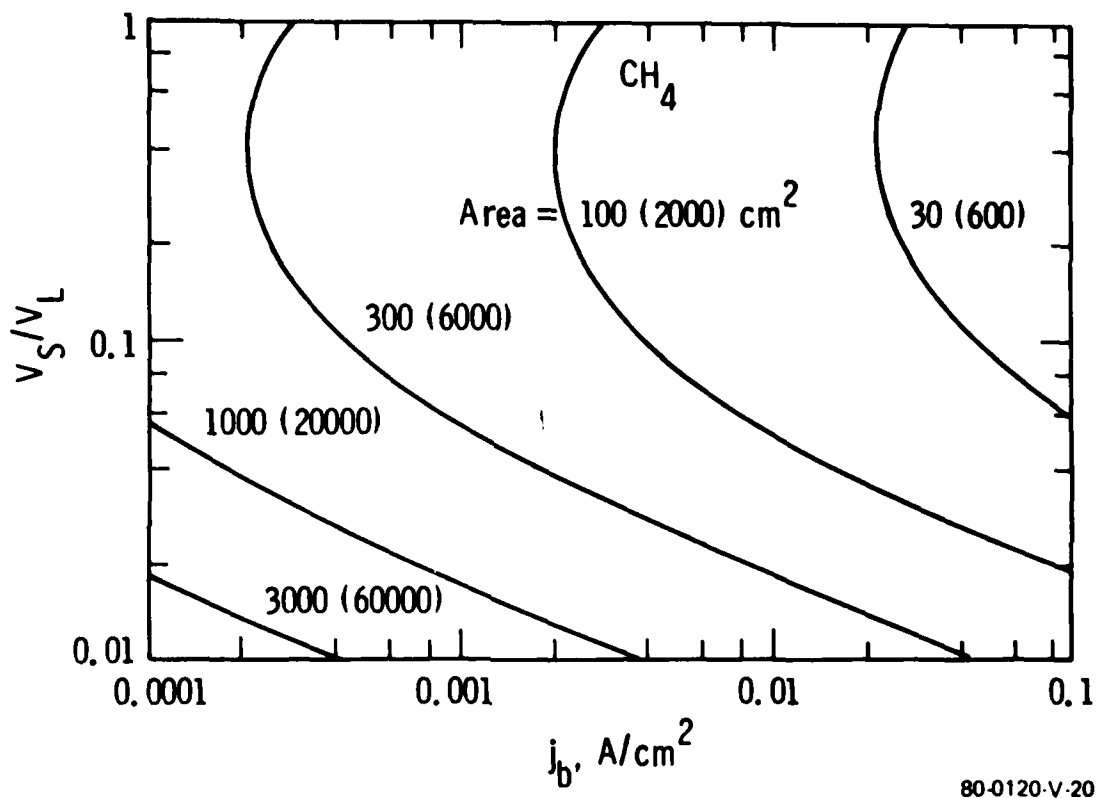
Figure 18. Switch Areas in Methane. The Area Required for a Current of 1kA is Given by the Values Next to the Curves. The Values in Parenthesis are the Areas Required for a Current of 20kA.

34
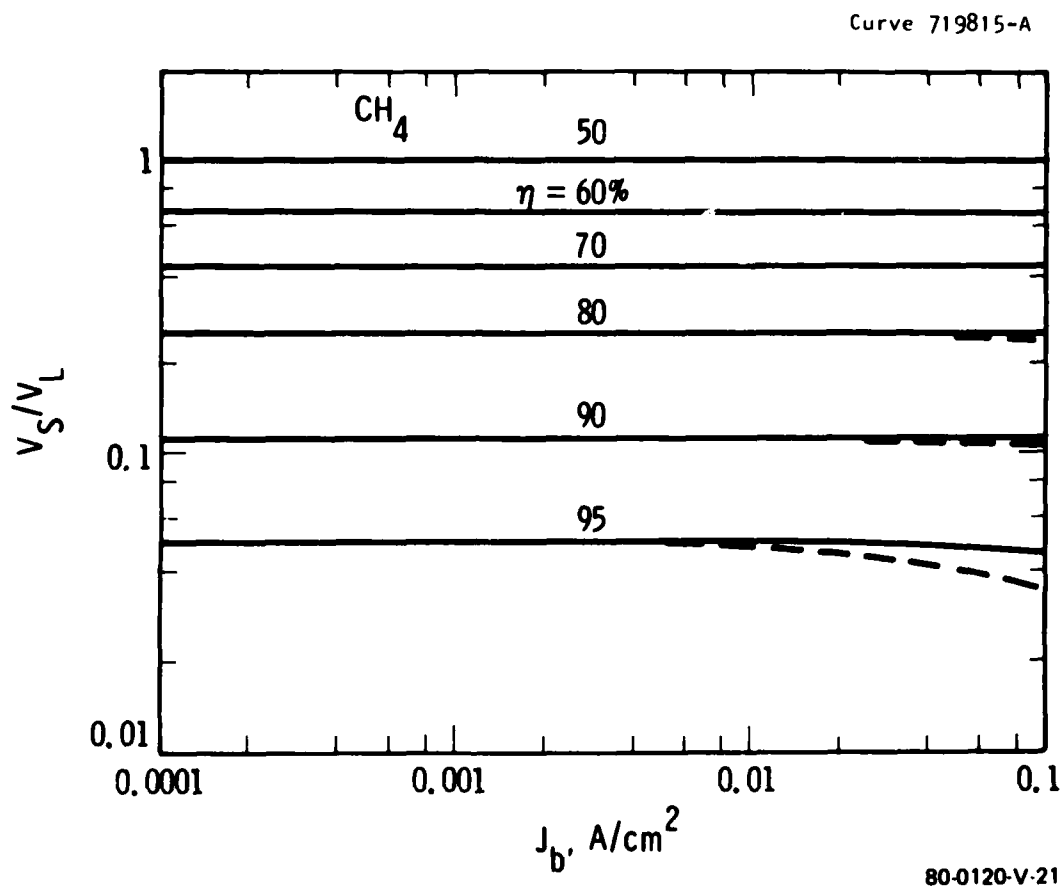
Figure 19. Switch Efficiency in Methane. The Solid Curves are for the V_p=100kV, I=1kA Case. The Dashed Curves are for the V_p=33.3kV, I=20kA Case.

35

The area required to carry currents of 1kA and 20ka is plotted in figure 18. The area required to carry a given current in methane is less than the area required to carry the same current in any of the gases studied previously. Contours of constant switch efficiency are given in figure 19.
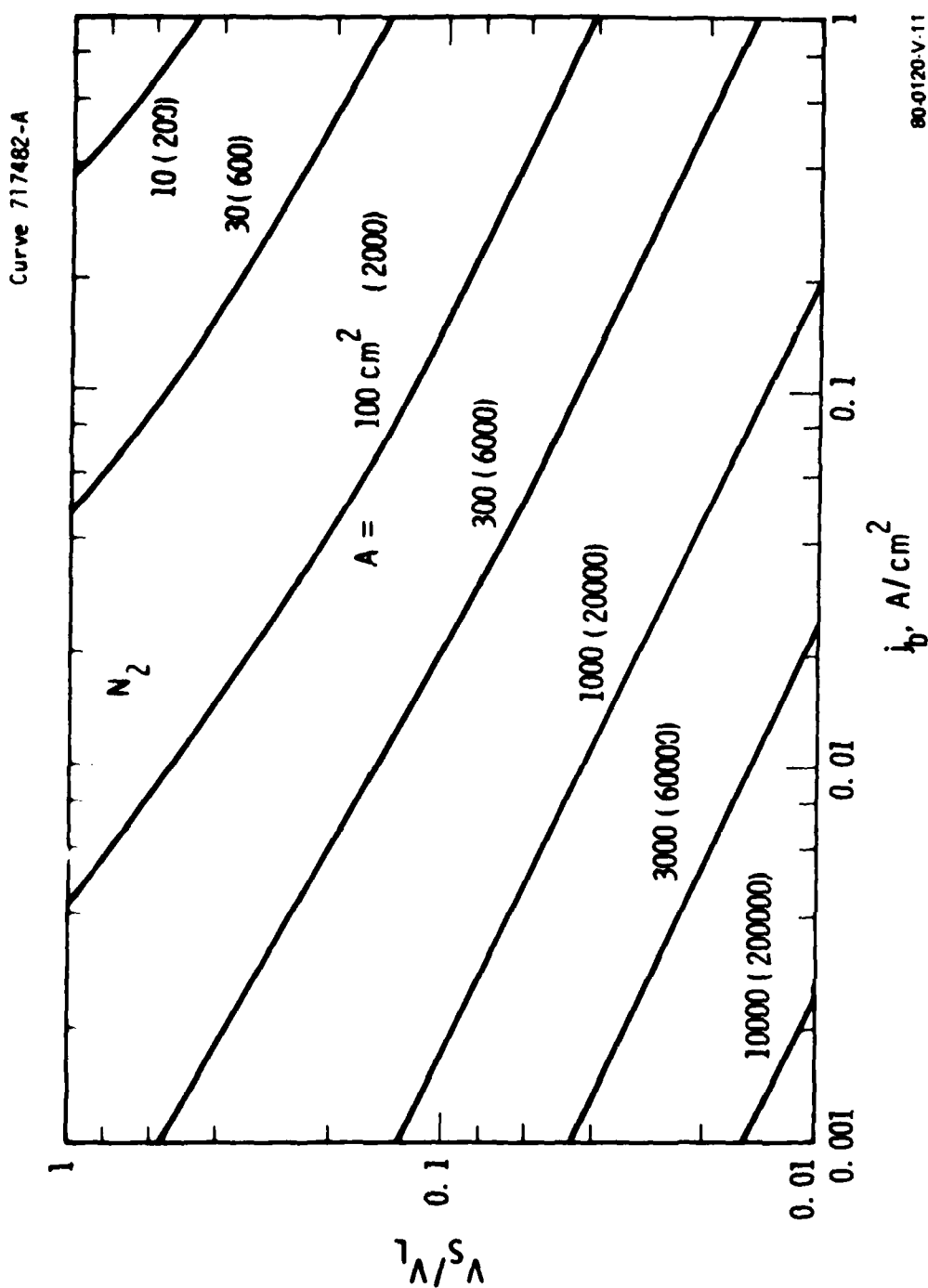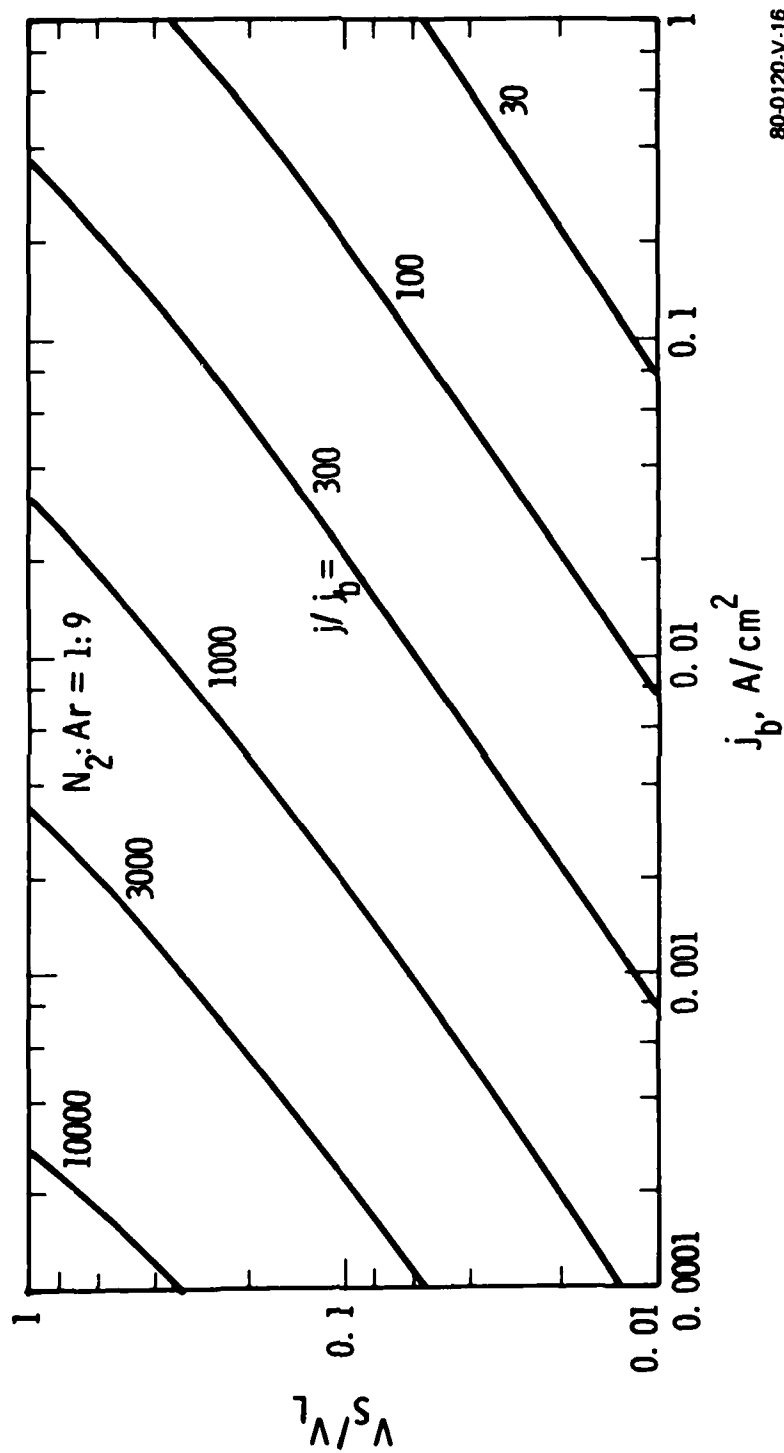
The switch properties shown in figures 17, 18, and 19 are quite attractive. These characteristics permit a more compact switch than is possible with the other gases (N_2, Ar and N_2:Ar= 1:9) studied. The attractiveness of methane for application in an e-beam ionized switch has been noted previously by Hunter[3] who performed a series of experiments using a laser discharge apparatus. We compare our theoretical predictions with Hunter's experimental results in section 2.3.3.

2.3.2 Approximate Steady Characteristics and Attachment Effects

The results presented in figures 8 through 19 suggest the following analysis which leads to approximate analytical predictions of switch performance. First we note that in the high current gain regime of interest ($j/j_b \geq 1000$) the energy dissipated in the switch discharge is much greater than the energy dissipated in producing the electron beam. In addition, the use of curve fits for W and k_r, as discussed above and summarized in table 1, suggested that an analytical approach was feasible.

We obtained an expression for j vs. E/N in the switch discharge by substituting equations (17), (20), and (11) into equation (12). Since attachment is either not present or negligible under steady-state conditions we set $\nu_a = 0$. The resulting expression is:

$$ j = A \, (E/N)^B \, q_e \sqrt{\frac{N \, g \, j_b}{E(E/N)^F}} \qquad \ldots\ldots\ldots \text{(23)} $$

Division of both sides by j_b and rearrangement gives:

$$ E/N = \left[\frac{(j/j_b) \sqrt{E}}{A \, q_e \, \sqrt{g}}\right]^{(\frac{2(0.5)}{B-0.5F})} \, N^{-(\frac{0.5}{B-0.5F})} \, j_b^{(\frac{0.5}{B-0.5F})} \qquad \ldots. \text{(24)} $$

36

or, defining T and S by comparison with Equation (24):

$$E/N = (T^2 j_b/N)^S \qquad \dots\dots\dots \quad (25)$$

Finally, substituting $V_s = 1 \times 10^{-17}$ (E/N) Nd into equation 25 gives:

$$V_s = 1 \times 10^{-17} (T^2 j_b/N)^S \text{ Nd} \qquad \dots\dots\dots \quad (26)$$

The switch area required to carry a total current at a fixed-current gain is simply:

$$A = I (j/j_b)^{-1} j_b^{-1} \qquad \dots\dots\dots \quad (27)$$

We evaluated equations (26) and (27) for the four gases studied with the results shown in figure 20. The calculations were done for the $V_p = 100kV$, I = 1kA case using the value of A,B,E, and F given in table 1 and the values of N and d from table 3. The current gain is fixed at $j/j_b = 1000$ for each curve. Note that since both I and j/j_b are fixed, the required area is the same for all four cases and is simply inversely proportional to the e-beam current density. The curves of V_s vs. j_b again show that methane is the best gas studied, with the N_2:Ar=1:9 mixture next, and N_2 and Ar least suited for use in an e-beam switch. The validity of the approximation given by equation (26) can be assessed by comparing the approximation for methane, given by the solid line, with the corresponding numerical results, given by the dashed curve.

We have also obtained approximate analytical expressions for the current gain which are valid in the two limiting cases where 1) recombination is negligible and 2) attachment is negligible. In the first limiting case equation (1) gives:

$$n_{e_0} = S/\nu_a \qquad (28)$$

Substituting n_{e_0} from equation (28) and S from equation (16) into equation (11) gives (neglecting the ion terms):

$$j = I/A = j_b \text{ Ng } q_e \text{ W} \qquad (29)$$

Therefore, the expression for the current gain is

$$j/j_b = q_e \text{ g } (W/k_a) \qquad (30)$$

where $k_a = aW/N$ and W/k_a are functions of E/N. If the expression W/k_a goes through a maximum in the E/N range relevant-to-switch operation, then j/j_b will have a maximum value. We have evaluated
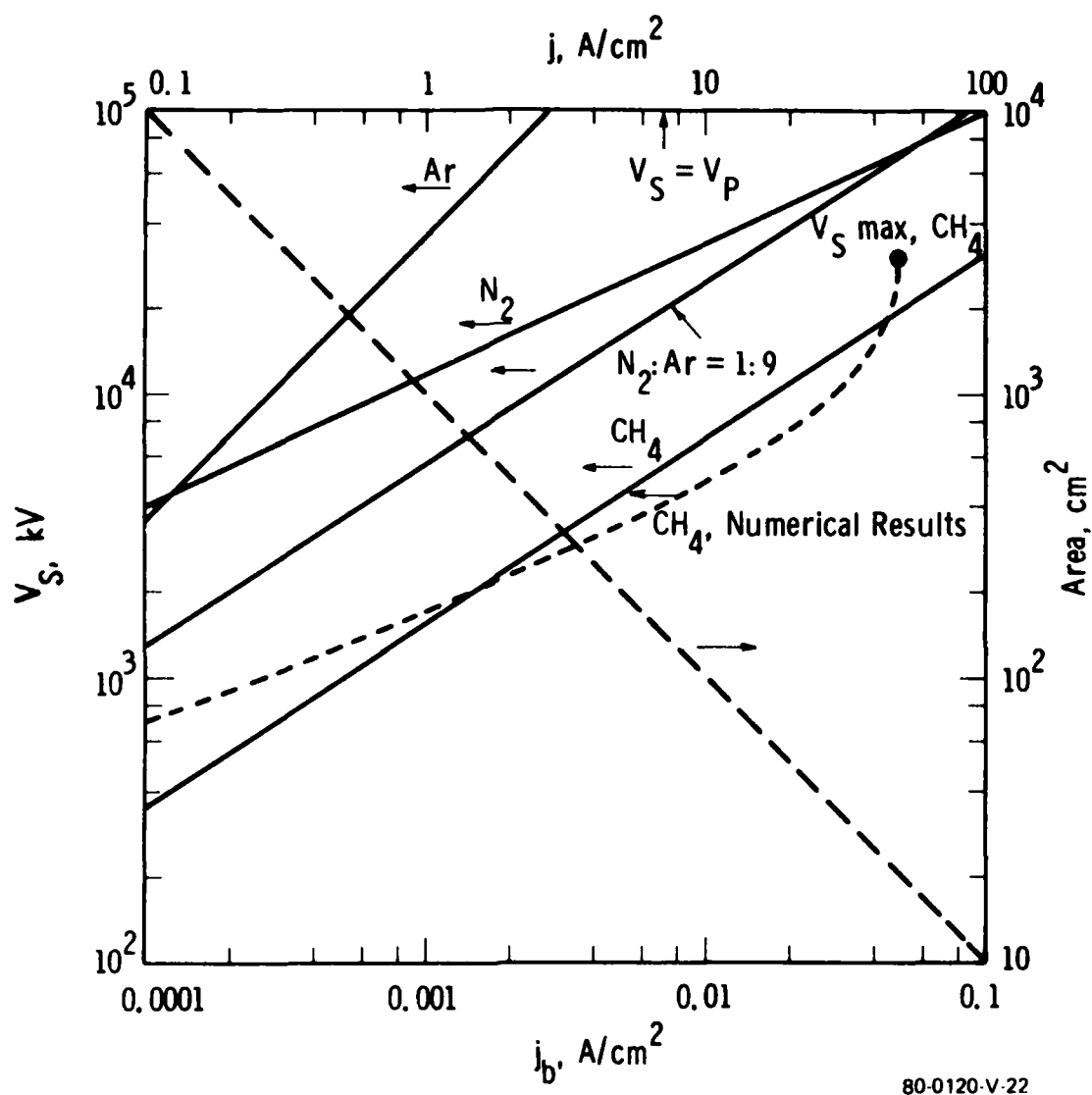
Figure 20. Approximate Analytical Switch Characteristics for a Fixed-Current Gain $j/j_b = 1000$ and a Fixed Total Current of 1kA.

equation (30) for methane. We assumed constant k_a values representative of an impurity attacher. When k_a is constant, W/k_a goes through a maximum since W goes through a maximum. The calculated values of (j/j_b) max are plotted vs. k_a in figure 21. The maximum attainable current gain falls to rather small values with relatively small values of k_a. Therefore, high gain is possible only with non-attaching or weakly attaching gases. The k_a scale in figure 21 refers to the total gas density. However, this figure also can be used to estimate the effect of attaching impurities. For example, for strong attachers such as SF_6, $k_a \sim 1 \times 10^{-9}$ referred to the SF_6 pressure. Hence, an SF_6 impurity of 40 ppm (effective $k_a = 4 \times 10^{-14}$) will limit the current gain to 1000. Attachment also increases the switch voltage as discussed below.

In the limiting case where attachment is negligible, the expression for the current gain is:

$$j/j_b = q_e \sqrt{Ng/j_b} \quad (W / \sqrt{k_r}) \tag{31}$$

where the expression $w/\sqrt{k_r}$ is again a function of E/N. This expression also has a maximum value in methane so that j/j_b also goes through a maximum in methane in this limiting case. The maxima are evident in figure 17. Since j_b and N appear in equation (31) the maximum current gain varies as j_b and N vary, in contrast with the attachment dominated limit. We have evaluated equation (31) for the values $N = 1.08 \times 10^{20}$ cm^{-3} and $j_b = 1 \times 10^{-4}$ and 0.1 A/cm^2. The resulting $(j/j_b)_{max}$ values are plotted in figure 21. The limits given by equations (30) and (31) are good approximations in the sense that they define the maximum value of j/j_b rather accurately over most of the parameter range that we have studied numerically.

We have also studied the effect of attachment on the steady-state switch characteristics by numerically calculating V_s vs. j_b curves for various values of k_a. These curves were determined by plotting j/j_b vs V_s curves for various j_b values and fixed k_a values. These curves were then used to determine V_s vs j_b for a
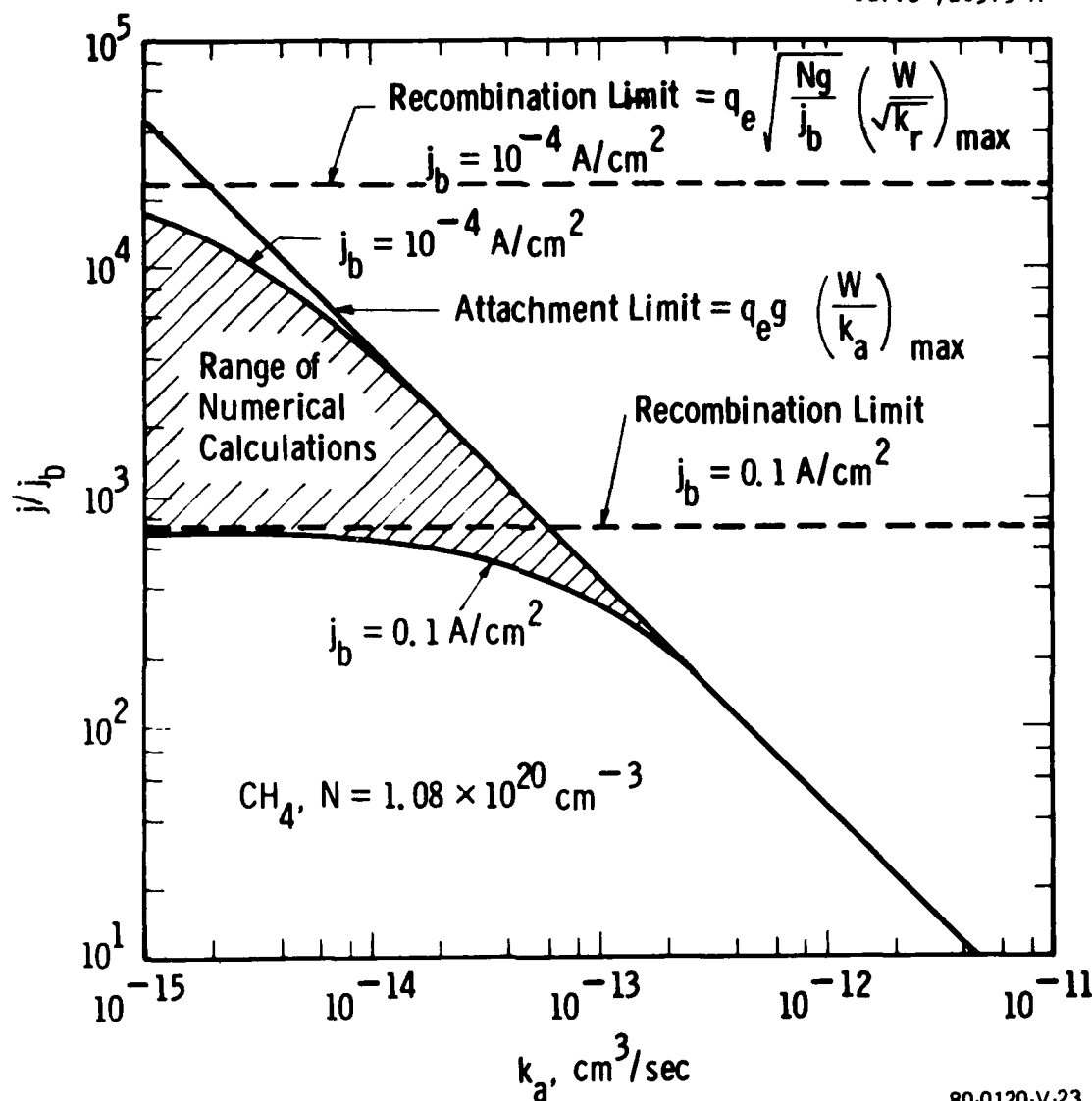
Figure 21. Maximum Current Gain Vs. the Two-Body Attachment Rate
Coefficient. The Lines Are Analytical Limits. The Shaded
Region Gives the Result of the Numerical Calculations

fixed value of j/j_b. The resulting curves are shown in figure 22 for four values of k_a. Note that the switch voltage is strongly affected by rather small k_a values. Hence, only nonattaching or weakly attaching gases are suitable for e-beam switches, and attaching impurities must be carefully controlled.

2.3.3 Transient Characteristics

We have done a series of transient calculations in order to predict the turnon and turnoff times for electron-beam ionized plasma switches. The results of the transient calculations confirm the assumption, made in the steady-state calculation, that equation (11) can be used to predict steady-state electron densities.

The first transient calculations were performed for the experimental conditions of Hunter[3] who studied e-beam discharges in methane. Hunter's experiments are interesting because they were performed to assess the idea of using an e-beam discharge as a switch. The physical size of the device used by Hunter is reasonable, and the total current and hold-off voltage are similar to regime 2 of table 2. In addition, the power dissipated in the switch is only ~ 2 percent of the power dissipated in the load. However, the e-beam power is identical to the power delivered to the load because a high-voltage, high-current density e-beam was used. Hence, the specific experimental conditions of reference 3 are not of practical interest except in special situations where an inefficient switch can be used. Nevertheless, we have simulated these conditions in order to test our model and the transport data that we have used for methane.

The experimental conditions assumed[3] are listed in table 4. The results of the calculations are shown in figure 23. The predicted rise in n_e, and the corresponding rise of the switch current and fall of the switch voltage is very rapid. Steady-state conditions are reached in ~50 ns. The predicted voltage collapse and current rise are much faster than the observed voltage collapse and current rise, suggesting that the circuit inductance plays a dominant role in Hunter's experiments.

41
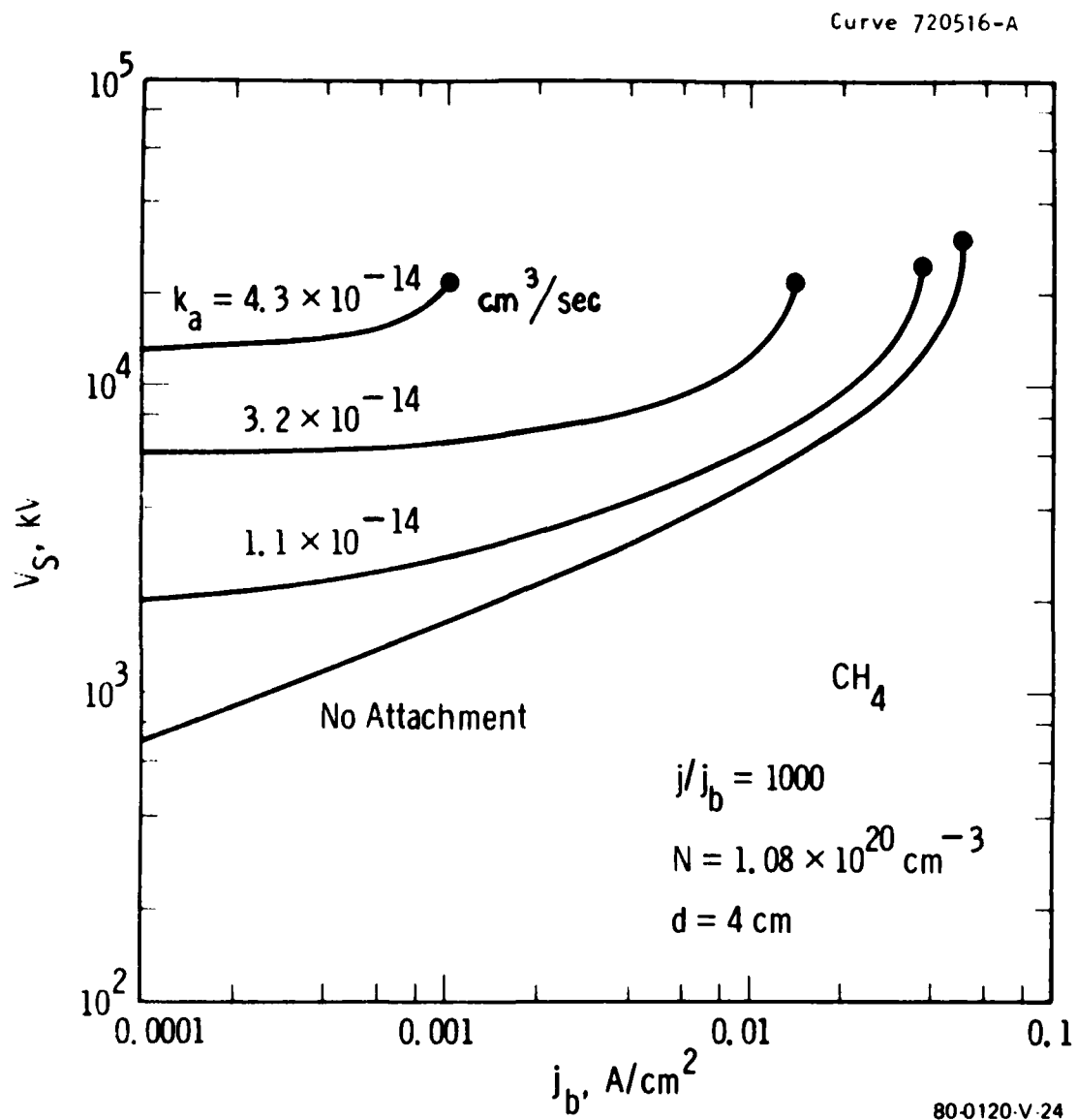
Figure 22.   Calculated Curves of V_s vs j_b for Four Different
Values of the Attachment Coefficient
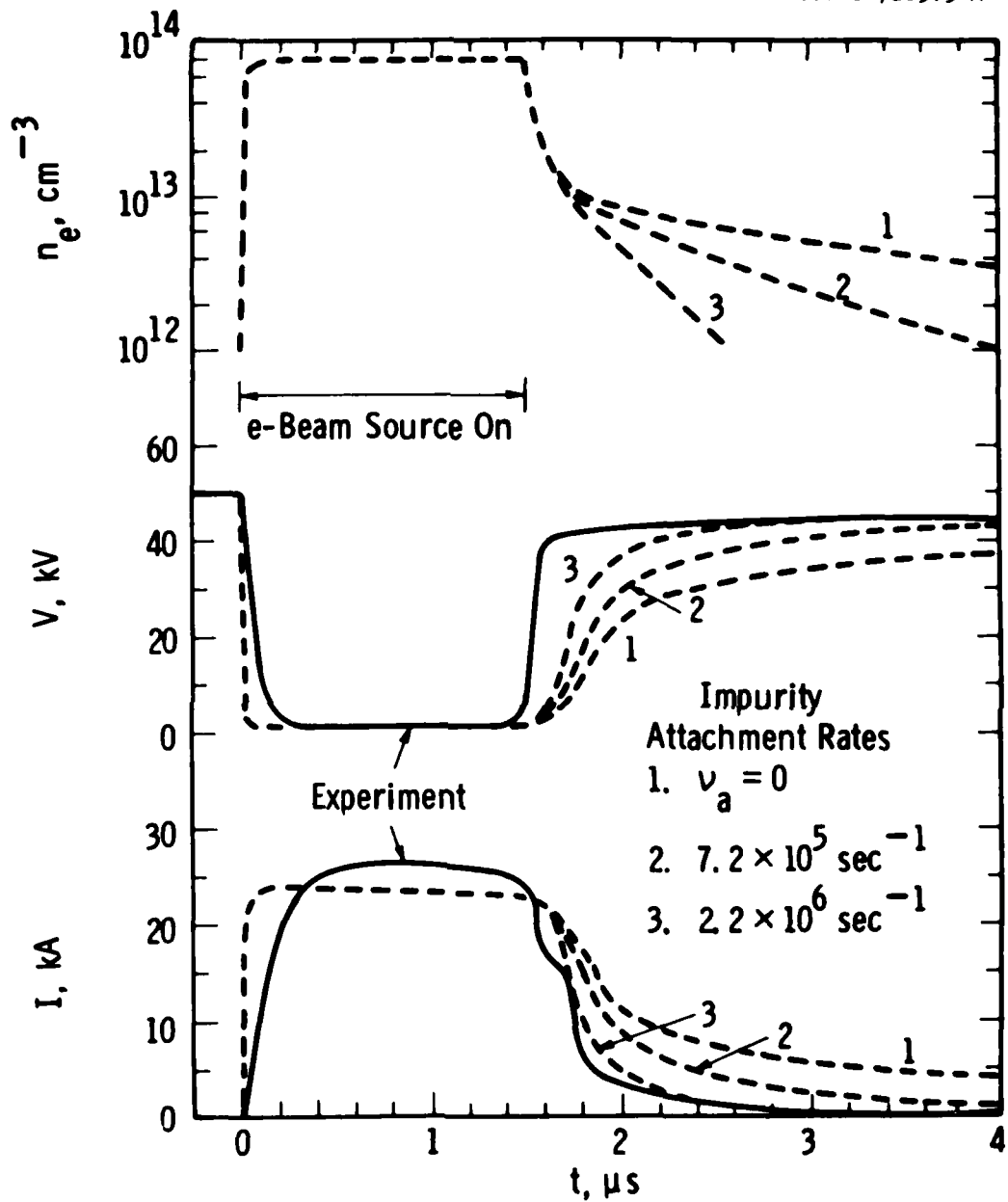
80-0120-V-24

Figure 23. Measured and Predicted e-Beam Switch
Waveforms in Methane

43

TABLE 4

PARAMETER VALUES ASSUMED IN THE SIMULATIONS OF THE EXPERIMENTS OF REFERENCE 3

Area	1000 cm^2
Gap Length	10 cm
Gas Density	$2.69 \times 10^{19} \text{ cm}^{-3}$
V_p	50 kV
R_L	$2 \, \Omega$
C	$9 \, \mu\text{F}$
i_b	5 A/cm^2
V_b	250 keV
S (calculated)	$2.35 \times 10^{21} \text{ cm}^{-3} \text{ sec}^{-1}$

80-0120-V-25

The predicted quasi-steady-state switch voltage and current values are in approximate agreement with Hunter's measurements, suggesting that the predicted steady-state n_e value is in approximate agreement with experiment. The current falls during the switch conduction period because the power supply capacitor voltage falls from 50 kV at t = 0 to 46.1 kV at t = 1.5 μs.

The predicted current fall and voltage recovery for the curves labeled "1 - no impurity attachment" is much slower than the observed current fall and voltage recovery. The predicted switch turnoff is slow because the only significant electron loss is recombination. The attachment rate due to methane is negligible in the E/N range corresponding to these experimental conditions with ν_a 1 x 10^5 at the highest E/N and $\nu_a \sim 0$ during most of the switch turnoff time. Better agreement with experiment can be obtained by adding an additional attachment loss. Two additional calculations were performed with constant attachment loss rates

44

of 7.2×10^5 cm sec^{-1} and 2.2×10^6 cm sec.$^{-1}$ The predicted waveforms are in better agreement with the experiment, as shown in figure 23. It should be noted that the circuit inductance is neglected in the calculations. If the circuit inductance was included, the predicted voltage waveform would rise faster during switch turnoff, but the predicted current waveform would fall more slowly. Comparison of the measured and predicted results in figure 23 suggests that either the methane attachment rate calculated from the cross section of reference 20 is too low or that an additional attachment process due to an impurity was present in the experiments of Hunter.

We have also calculated transient switch characteristics for the N_2:Ar = 1:9 mixture and for methane for some of the same experimental conditions as in the steady-state calculations described in section 2.3.1. The parameter values assumed are given in table 5.

TABLE 5

PARAMETER VALUES ASSUMED IN THE TRANSIENT
CALCULATIONS FOR A N_2:Ar = 1:9 MIXTURE AND FOR METHANE

	N_2:Ar = 1:9	Methane
Area	500 cm^2	200 cm^2
Gap Length	5 cm	4 cm
Gas Density	8.07×10^{19} cm^{-3}	1.08×10^{20}
V_p	100 kV	100 kV
R_L	91 Ω	95 Ω
J_b	2 mA/cm^2	5 mA/cm^2
V_b	100 keV	100 keV
S (calculated)	7.3×10^{18} cm^{-3} sec^{-1}	1.54×10^{19} cm^{-3} sec^{-1}

The predicted electron density, switch voltage and switch current are shown in figure 24. The rise time of n_e and I, which are controlled by the values of S and k_r is ~ 2 μsec for the case studied. However the switch turnoff time when recombination is the only electron loss is quite long (>30 μsec) as shown in figure 24. This behavior is typical of the electron density decay which occurs due to recombination. Significantly faster turnoff times with recombination alone could be obtained only by using heavy molecular species which have high recombination rates and a small variation of recombination rate as electron temperature increases. Even with such species, the electron density will decay less and less rapidly as time increases as is characteristic of a recombination decay.

Faster switch turnoff can be obtained by adding an attaching species to the gas mixture used in the switch. However, too much attacher will reduce the value of n_{eo} with a corresponding reduction in the switch efficiency as discussed above. We have made a calculation where we added 1 m Torr of SF_6 to the N_2:Ar = 1.9 mixture (at 2280 Torr, 273^ok or 3 amagats) with the results shown in figure 24. This small amount of SF_6 does not significantly change the values of n_{eo}, V_s and I, but the switch now turns off in ~ 10 μsec. Similar results could be obtained with a larger quantity of a weaker attacher.

The final transient calculations were performed for methane. The results are shown in figure 25. The switch turnoff is again quite slow in pure methane, even though methane has a weak dissociative attachment process, because the small attachment rate due to this process has a negligible effect. The addition of a small amount of an impurity with a resulting attachment rate of ~ 1 x 10^6 sec^{-1} has a dramatic effect, as shown in figure 25, giving a turnoff time of ~ 2 μsec.

The results shown in figures 24 and 25 suggest that a small attachment loss is essential in order to achieve a turnoff time in the desired 1-10 μs range.
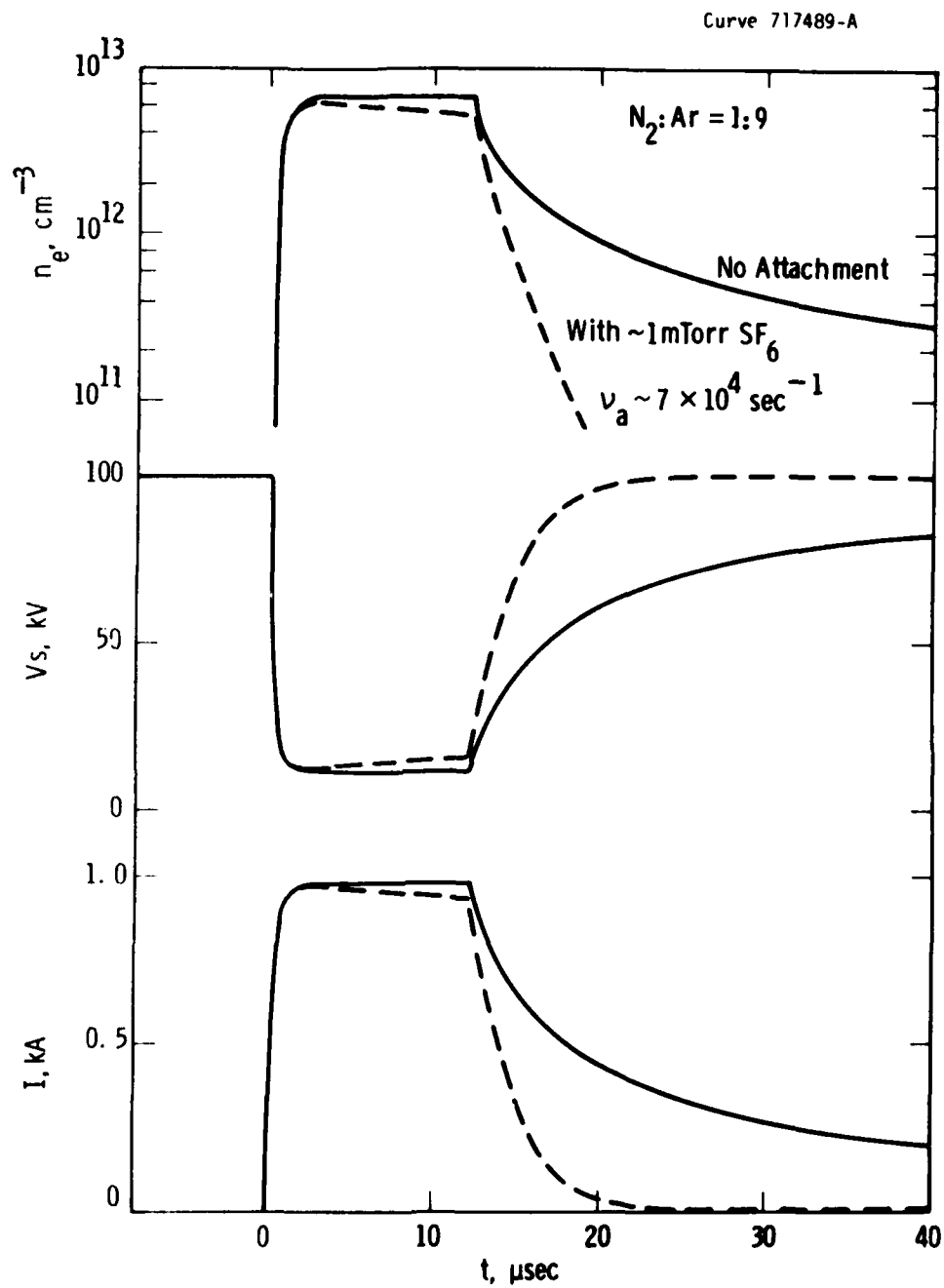
Figure 24. Predicted Transient Characteristics for a
N_2:Ar = 1:9 Mixture With and Without 1m Torr of SF_6

47
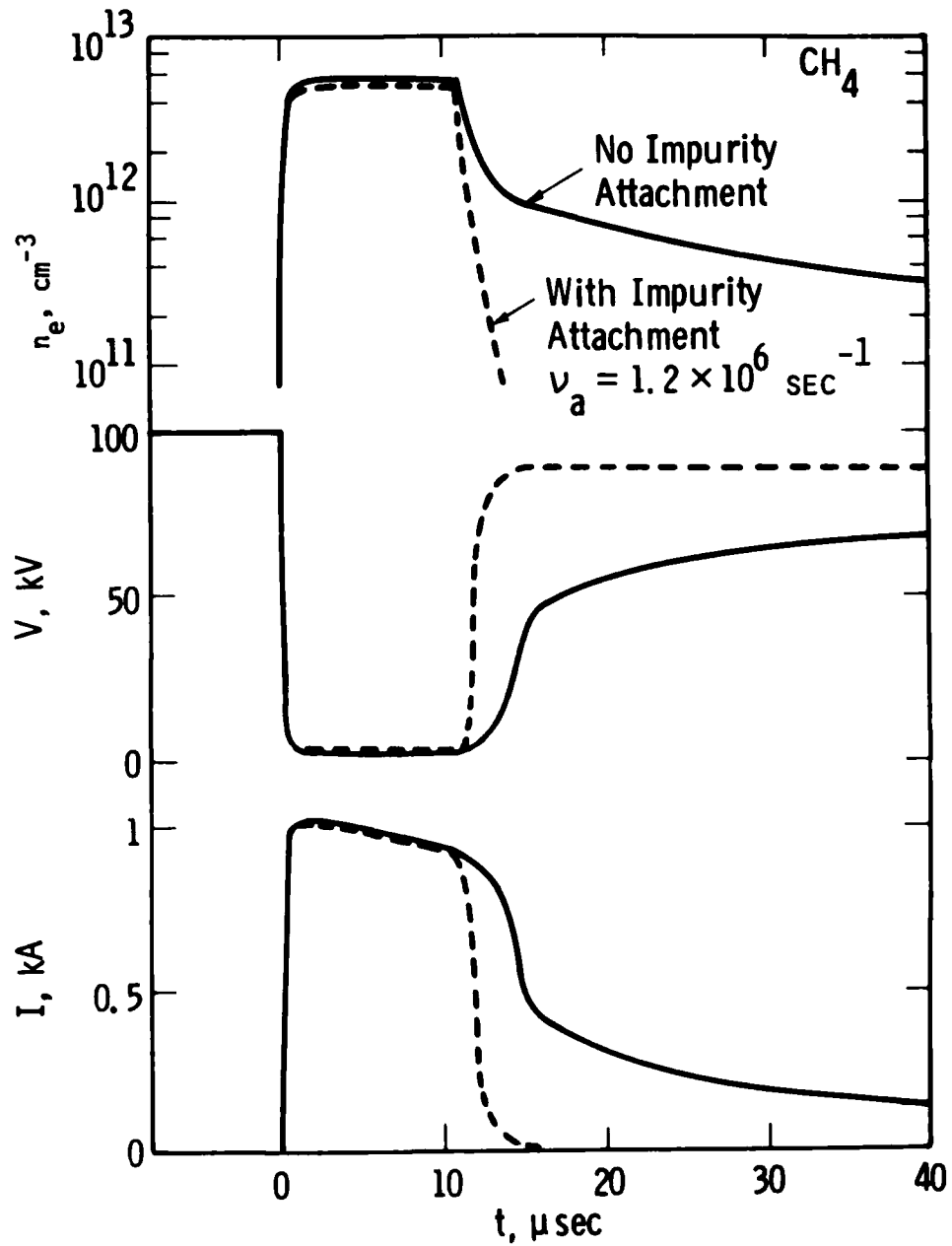
Figure 25. Predicted Transient Characteristics for Methane
With and Without a Small Amount of an Attaching Impurity

48

The calculated gas temperature rise at the end of the 10 μs on time of the switch is only 2.5°K for the conditions of figure 25. The temperature rises an additional 2.5°K during switch turnoff in the case where $\nu_a = 1.2 \times 10^6$ sec^{-1}. The gas temperature continues to rise during the entire 40 μsec of the simulation in the case where no impurity attachment is present and reaches a final temperature of 339°K (39°K temperature rise). These small values of temperature rise suggest that a very slow gas flow rate will be adequate for the conditions of figure 25.

For the case where pulses of 10 μs duration are switched at a 1000 Hz rate, the temperature would rise 2500°K during on-time and at least an additional 2500°K during switch turnoff. Under static-gas conditions, such a temperature increase would lead to thermal instability. Considering the switch geometry presented later in figure 28 where the discharge is approximately 5.4 cm wide in the direction of gas flow, a gas velocity of 55 meters per second would be adequate to provide clearing of the switch gap between pulses and reducing the temperature rise in the discharge gap to the previously indicated value for a single 10 μs pulse. The velocity of sound in CH$_4$ at 0°C is 432 meters/ sec. Thus, reasonable subsonic gas velocities would be required. In the case of a single 500 μs pulse, a 120°K temperature rise would occur during the on-time which does not pose a thermal stability problem. As only a few 500 μs pulses per second would be permitted, a low gas flow rate will be adequate to maintain stable conditions. In the 20kA switch, a heat loading 2.5 times that used in the 1kA switch would occur if a 4000 cm^2 discharge area is used. Increasing the gas flow velocity by a factor of 2.5 times that used in the 1kA switch would still give reasonable achievable gas flow velocities.

The calculated buildup of dissociation products for the conditions of figure 25 reaches a level of about 10^{11} cm^{-3}. This is a very small degree of dissociation since the total gas density is about 10^{20} cm^{-3}. In fact, the predicted total dissociation at

10^6 pulses is only about 0.1 percent, even in a static system where the total gas volume is equal to the discharge volume. The results of this dissociation calculation suggest that gas dissociation can be neglected in an e-beam switch which has a low discharge E/N, as is the case for the calculation of figure 25. For the case of 500 μs pulses, the total dissociation after 10^6 pulses will be about 5 percent in a static system. At this level of dissociation, some provisions for gas conditioning will be needed to maintain design characteristics of the switch over the required duration of operation.

2.4 EXTERNAL IONIZATION SOURCE

The type of external ionization source selected for the high-voltage switch using externally ionized plasmas should be the one which offers the greatest potential for a large ratio of switched power to control power. Electron-beam ionization of gases has been shown to be the most efficient, with achievable ionization efficiency of at least 50 percent.[39] Because of this, the intent of this study was to use electron-beam ionization; however, initial cursory consideration was also given to UV, X-ray, and laser source for the sake of completeness. All these sources are much lower in overall efficiency then e-beams for producing a uniformly ionized plasma in a volume.

UV photoionization-produced plasmas have been reported in the literature as an alternate to e-beam external ionization with the principal advantage being the elimination of the thin foil window between the high-pressure discharge chamber and low pressure e-beam source. However, the overall UV photoionization energy efficiency demonstrated has been low, less than 1 percent for spark-gap UV sources. Conversion efficiency of electron-beam energy into fluorescence output of argon[40] at 126.1nm has been shown to be as high as 10 percent. This experiment required 600 to 1000 psia argon gas pressure in a chamber with a 0.01 cm thick titanium foil window. An electron beam of 800 - keV electrons in 60-ns pulses was used to excite the fluorescence which was transmitted outside through a MgF_2 window. This type of UV source possesses all the disadvantages of electron-beam plasma excitation plus that of lower efficiency and the need for low ionization seedant in the switch gas to more effectively couple with the UV photons. Higher fluorescence efficiencies[41] have been measured in other gases at longer wavelengths, but these wavelengths are not considered suitable for use as an external ionization source.

Several papers have appeared[42,43] discussing X-ray preionization for electric discharge lasers. The efficiency for generation of X-rays from electrical energy is notoriously poor. X-rays

51

do not appear to be competitive for producing a sustained plasma compared to e-beam or UV. Radioactive isotope sources of ionizing radiation suggest themselves. However the required shielding, slow mechanical shuttering for turning the radiation "on" and "off," and the safety and legal restrictions do not make the radioactive isotope approach attractive.

Laser-induced discharge phenomena have been studied and discussed[44] to a considerable extent. The low efficiency for electrical-to-laser radiation conversion coupled with the poor absorption of laser energy for gas ionization, does not recommend laser radiation as a means for producing an externally ionized plasma in a switch.

Electron-beam sources considered consisted of thermionic, cold cathode, field emission, and a special case of field emission utilizing a thin-film microstructure cathode that functions at relatively low voltages. Thermionic e-beam guns represent a standard technology with considerable experience from the vacuum tube industry providing design and performance parameters. For the application considered in this study, a thermionic electron source suffers from relatively long turnon time (time for emitter to heat up to and stabilize at working temperature), requires substantial heating power, produces radiated infrared energy which applies an additional heat load on the thin-film window, thus lowering the electron-beam loading it can transmit, and is not the best type of source for producing a uniform electron density over an extended area.

Cold cathode e-beam guns of two types,[45] plasma-cathode electron gun and ion-plasma electron gun, have been studied as non-thermionic electronic guns with properties suitable for application to e-beam sustained or controlled lasers. These studies have demonstrated cold cathode sources with up to 1000 cm^2 apertures, with relative insensitivity to contamination, with fast turnon capability and relatively good beam uniformity over the gun aperture. Initially one of the cold cathode e-beam guns was being

52

considered as the choice for controlling the high voltage switch using an externally ionized plasma. However, as the study progressed it was found that higher control gain and a simpler gun mechanization made the thin-film field emission cathode the preferred choice.

Standard field emission cathodes consisting of needle-shaped field emitters or razor blades have been used extensively to provide high-power pulsed electron beams with applications in nuclear fusion studies, radiation physics, production of X-rays and pumping of gas lasers. The field emission emitters require high applied voltages ranging from many tens of thousands to hundred of thousands of volts to produce the needed high fields and desired emission current levels. As such, they offer bulky electrical mechanization, would offer low control power gain for e-beam plasma switch, are subject to diode closure problems for long pulses, and are difficult to make with identical field conversion factors or repeatable performance from array to array. The standard field emission electron source does not recommend itself for use in the e-beam plasma switch.

A special case of field emission resulting from a thin-film microstructure cathode[46,47] was studied because of the unique advantage it offered. It was found that the thin-film field emission cathode offered a means of controlling a switch using externally ionized plasma with a very high power gain. This field emitting cathode runs at only 100 to 200 volts which is a voltage level that is compatible with power transistor circuitry. As the electrons are emitted almost instantly after the cathode voltage is turned on, switching of the electron beam "on" in well less than a microsecond is possible.

The thin-film field emission cathode is built using solid-state technology similar to that used for metal-oxide semiconductor devices. A cross section of a single point field emitter is shown in figure 26. In actual practice many of these field emission cathodes can be fabricated per square centimeter of silicon wafer

MOLYBDENUM
GATE FILM

0.4 μm

1.5 μm

1.5 μm

SILICON
DIOXIDE
INSULATING
LAYER

MOLYBDENUM
CONE
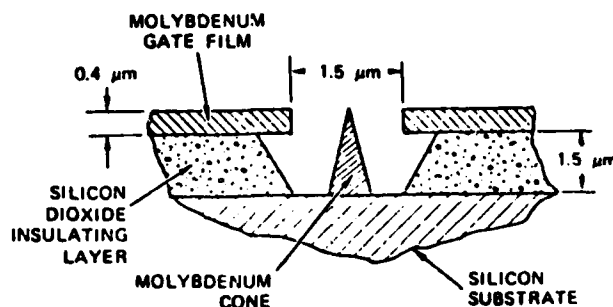
SILICON
SUBSTRATE

80-0120-V-30

Figure 26. Cross Section Diagram of a Thin-Film Field Emission
Cathode (Taken from Reference 46, Figure 1)

to achieve rather high total currents. As shown in figure 26,
the cathode structure consists of a molybdenum (Mo), silicon
dioxide (SiO_2), and silicon (Si) sandwich. Fabrication starts
with a heavily doped silicon wafer (0.01Ωcm). A summary of suitable
fabrication steps is listed below:

(a) Steam oxidize wafer to about 1.5 μm thickness.

(b) Coat the oxide with a uniform layer 0.4 μm thick molyb-
denum in an electron beam evaporator.

(c) Coat molybdenum layer with a photoresist using spinning
method.

(d) Expose resist-coated surface to 1 μm diameter dot pattern.
Either an electron beam or an optical projection system can be
used.

(e) Develop resist to from open areas corresponding to the
1 μm dot exposure.

(f) Selectively etch the molybdenum through to the silicon
dioxide.

54

(g) Remove the remaining resist. Then etch the silicon dioxide down to the silicon substrate with a buffered hydrofluoric acid solution. The molybdenum layer is undercut by etching of the silicon dioxide, since the oxide etch does not attack molybdenum.

(h) Mount the substrate in a vacuum deposition system and rotate the substrate about an axis perpendicular to its surface. A parting layer of aluminum is deposited at grazing incidence. In this way the size of the hole can be decreased to any desired diameter. Also the aluminum serves as a parting layer for the subsequent molybedenum evaporation.

(i) Deposit molybdenum through the partially closed holes by electron-beam evaporation from a small source at normal incidence. The size of the hole continues to decrease because of condensation of molybdenum on its periphery. A cone grows inside the cavity as the molybdenum vapor condenses on a smaller area, limited by the decreasing size of the aperture. The point is formed as the aperture closes.

(j) Dissolve the parting layer of aluminum, releasing the molybdenum film deposited during the cone formation step. After a thorough cleaning, the cathode is ready for use.

The above enumerated fabrication steps are typical of semiconductor fabrication operations that are subject to good control which permits the positioning of individual cones with high precision and provides the ability to pack large numbers of identical cones into small areas.

The major advantage offered by these thin-film field emission cathodes is the very low voltages at which they operate, typically from 100 to 200 volts. This low voltage operation is achieved by virtue of the accelerating electrode (molybdenum gate film) being close to the cone tip and by the radius of tip being very small (500 $\overset{\circ}{A}$). Also the low operating voltage of these cathodes makes them less vulnerable to sputtering damage by ionization of the ambient gas. This allows the cathodes to operate continously

with very stable emission properties and long life at pressures higher than those necessary for conventional field emitters. Experimental measurements[46] indicated that each individual tip can stably emit 20 μA of current. Spindt et al.[46] have fabricated square arrays of thin-film emitters on 12.7 μm centers which were capable of operating at effective current densities of greater than 10 A/cm^2 continously. For the high voltage switch using externally ionized plasma, limitation on electron-beam current density ranging from a hundred μA/cm^2 to a few mA/cm^2 is imposed by the requirement that switch current gain (I_{switch}/I_{e-beam}) to be at least 1000. (The current gain is high when the electron-beam current is small and the switch voltage is large). At these levels of current density, thin-film field emitter spacing of 500 μm in arrays of 400 emitters/cm^2 would be more than adequate to meet the current requirements. It may be noted that current density limitation resulting from the maximum allowable heat loading of the thin-film window is substantially greater than that imposed by switch current gain. The allowable electron-beam loading was estimated from information presented by Daugherty in Chapter 9 of reference 6. Assuming aluminum foil with support spacing of 1 cm and a $\Delta T \leqslant 200^\circ C$, for 10 μs pulses at 1,000 PPS the electron current limit was 50 ma/cm^2 and for 500 μs pulses at 1 Hz the limit was 120 ma/cm^2.

The plasma switch is turned "on" and "off" by turning the field emitter "on" and "off." The 100 kV acceleration of the e-beam is accomplished in a separate gun section which is held at a constant dc potential and is not modulated for on/off control. A calculation of overall control power gain for an e-beam plasma switch using a thin-film emitter cathode is shown in equation (32).

$$\text{Control Power Gain} = \frac{\text{Switched Power}}{\text{Control Power}} = \frac{V_c \, I}{I_{FE} V_{FE}} \qquad (32)$$

where V_c is the power supply voltage, I is the circuit current (figure 1), I_{FE} is the electron current emitted by the thin-film field emitters and V_{FE} is the actual voltage applied to the thin-film field emitters to produce I_{FE}. It should be noted that equation (32) does not take into consideration the total power supplied to the electron gun. Also it does not consider the capacitance of the thin-film field emission cathode and thus represents a static state. Assuming 400 emitters per cm^2 in a rectangular array, it is estimated that the capacitance loading can be held to about 1.15×10^{-10} F/cm^2 of cathode area.

We assume that:

1) $\frac{I}{I_b} = 1000$ where I_b is the actual electron beam current in-

troduced into the plasma, 2) 50 percent of the electrons emitted by the cathode are lost to obstructions resulting in $I_b = 1/2\ I_{FE}$, 3) The voltage V_{FE} necessary to produce I_{FE} is 200 volts. Substituting the above conditions into equation (32) gives control

$$\text{power gain} = \frac{V_c\ I}{\frac{2I}{1000}} \times 200 = 2.5\ V_c$$

Then for the 100KV/1KA switch operating regime the control power gain = 250,000 and for the 30KV/20 KA switch operating regime the control power gain is 75,000.

The high control power gain offered by the use of thin-film field emission cathode plus the relatively low voltages needed to control this type of field emission cathode provides an attractive approach for the external ionization source needed for the plasma switch. A schematic diagram of a possible switch configuration is shown in figure 27. Not shown are provisions for gas flow cooling/deionization which would be accomplished by flowing the gas mixture used through the switch volume transverse to the discharge direction. A closed-loop gas conditioning system would be used to conserve gas and extract heat.

It is recommended that the thin-film field emission cathode be the choice as the external ionization source for the high
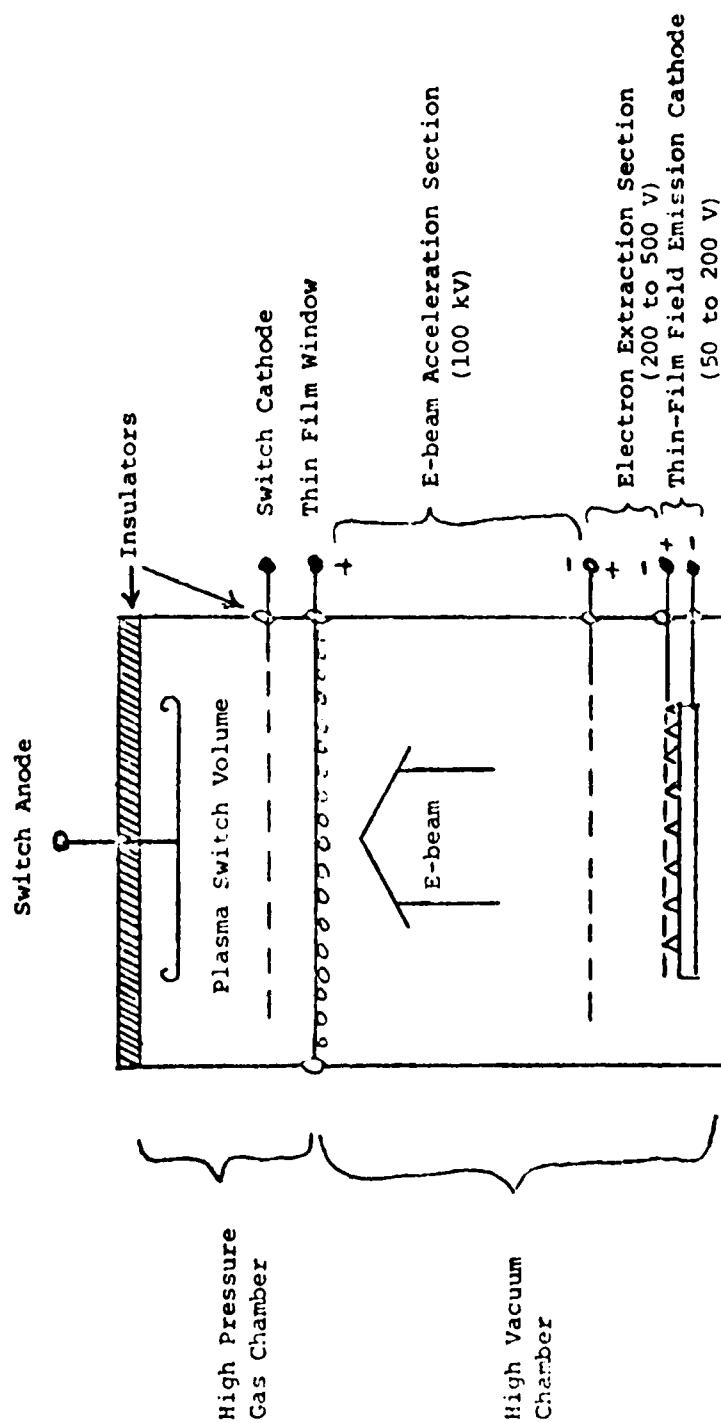
Figure 27. Schematic of a High-Voltage Switch Using Externally Ionized Plasma With a Thin-Film Field Emission Cathode

voltage switches using externally ionized plasmas. The high con-
trol power gain and the relatively low control voltage of the
thin-film field emission cathode provides a solution to the pro-
blem of controlling the e-beam and hence the plasma switch in an
efficient manner. Also this type of e-beam source provides an
electron emission uniformly distributed over an extended area
with the capability of being expanded or contracted simply as an
area function. Estimates of material and labor cost was $120
for 29 square cm of thin-film emission cathode area which would
be derived from a single 3-inch diameter silicon wafer. A suit-
able number of individual 29 square cm sections in a rectangular
array could be used to achieve the needed emitting area consis-
tent with the required discharge cross section.

The thin-film field emission cathode has been demonstrated
experimentally,[46,47] however, it is expected that further de-
velopment effort would be needed to establish a suitable capa-
bility for production of this type of electron source.

2.5 SWITCH GEOMETRY

The principal factors that need to be considered in defi-
ning the e-beam plasm switch geometry are:

- Switch Discharge Gap
- Discharge Area
- Gas Flow Cooling Deionization
- High Voltage Insulation
- Pressure-Vacuum Structures

The switch gap is determined by Paschen curves for the gas
used and depends on the hold-off voltage as a function of Nd.
The discharge area is determined by the switch current density
which is a function of current gain j/j_b and discharge voltage
drop V_s as shown in figures 9, 12, 15 and 18. The required
minimum j/j_b is 1000 and V_s for efficient switching must also
be a small percentage of the circuit voltage being switched,
typically less than 5 percent.

The heat generated in the plasma by the discharge current
can raise the gas temperature high enough to cause a sub-

instability leading to a glow-to-arc transition if the conduction
pulses are too long or the repetitive pulse frequency is too high
as noted in section 2.3.3. This situation can be circumvented
by use of gas flow in the direction transverse to the electric
current path. For a given transverse flow velocity, the pulse
repetition rate is limited by the rate of heat removed from the
discharge section. To optimize the effectiveness of the gas
flow to a minimum velocity, a rectangular discharge geometry is
desirable in which the width in the gas flow direction is short
compared to the other direction.

High voltage insulation requires that the electrode breakdown
distances to any electrically conducting structures be sufficient-
ly large to provide a substantial safety factor compared to the
minimum distance necessary to hold-off the voltage according to
Paschen curves. Also feedthrough insulators should have a rating
of at least 1.5 times the required switch hold-off voltage.

The operation of the e-beam source at a high vacuum and the
discharge chamber at 4 atmospheres absolute pressure of methane
requires that adequate consideration be given to the mechanical
strength of the pressure and vacuum structures, respectively.
Support for the thin-film aluminum (or titanium) window between
the two chambers should provide maximum transparency consistent
with adequate support for the foil. A schematic diagram showing
an exploratory mechanical mechanization for a 100 kV/1kA switch,
taking into consideration the above indicated factors, is shown
in figure 28. For the 30kV/20kA case, a similar configuration
is suggested with the dimensions adjusted to reflect a 1.33 cm
switch gap and a 4000 square cm discharge cross section. A closed-
cycle gas circulating and conditioning system is shown in figure
29 which would be used to conserve gas and provide the necessary
cooling.

2.6 COMPARISON OF DIFFERENT SWITCH TYPES

The comparison of different switch types was limited to
switches that have demonstrated controlled turnon and turnoff

60

TOP VIEW
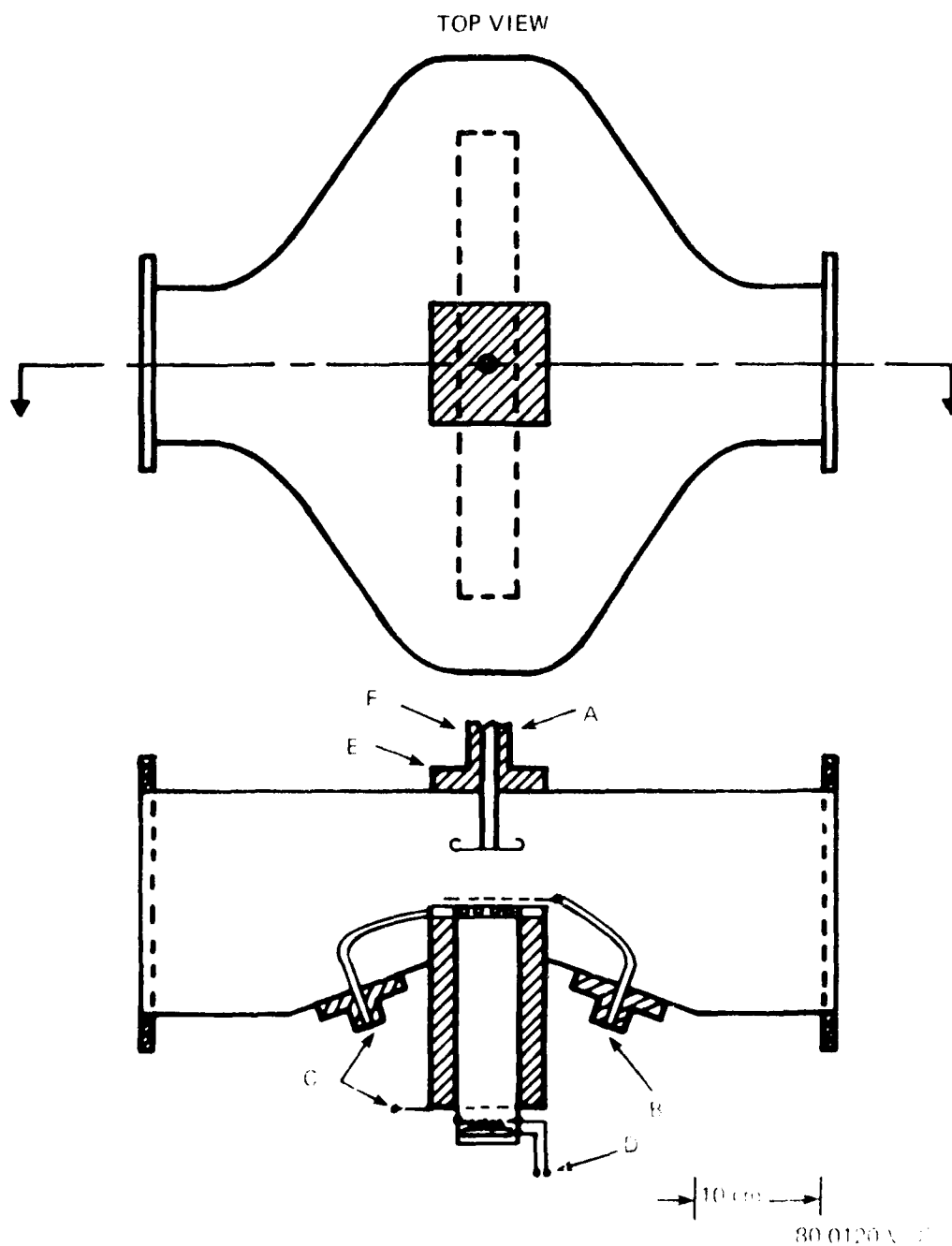
Figure 28. An Exploratory 100 kV, 1kA Plasma Switch Schematic Diagram. Discharge Cross Section 200 cm^2, Switch Gap d = 4 cm, A-Switch Anode, B-Switch Cathode, C-e-Beam Accelerator Terminals, D-Thin-Film Field Emission Cathode Connections, E-insulator, F-High Voltage Cable

61
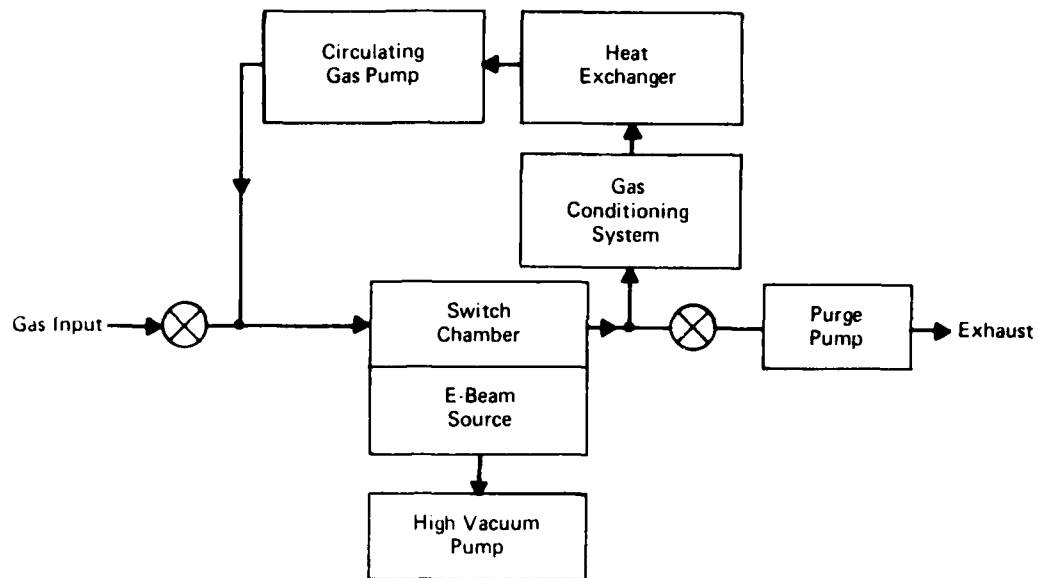
80-0120-33

Figure 29. Gas Flow Block Diagram of a Closed-Cycle Plasma
Switch Utilizing External Ionization

capability under the condition that voltage is applied continously.
Mechanical circuit breakers were not considered because their re-
sponse is too slow to meet the on/off and PRF requirements.
These constraints narrowed the number of candidates down to the
following four switch types:

- E-Beam Controlled Plasma Switch
- High Vacuum Triode or Tetrode
- Crossed-Field Switch
- Transistor Array

Specific comparisons were made at the two voltage and current
levels stated in the performance guidelines for the switch of
100 kV hold-off voltage/1kA on-current and 30 kV hold-off voltage/
20kA on-current. The results for the 100kV/1Ka case are summarized
in table 6.

For the e-beam plasma switch four discharge cross sections
were chosen to show the tradeoff between switch drop and size.
The switch characteristics were calculated for gas and circuit

62

TABLE 6

HIGH VOLTAGE SWITCHES WITH CLOSING AND OPENING CAPABILITY AT 1000 A, 100 kV HOLDOFF

Switch Type	Conduction Voltage Drop	On/Off Control	Control Power Gain	General Size Indication	Remarks
E-Beam Plasma Switch (CH$_4$ gas)	1300 1700 2300 3500	E-Beam Current: 5 $\times$ 10^{-4} A/cm^2 1 $\times$ 10^{-3} A/cm^2 2 $\times$ 10^{-3} A/cm^2 5 $\times$ 10^{-3} A/cm^2	250,000 250,000 250,000 250,000	2000 cm^2 1000 cm^2 500 cm^2 200 cm^2	Operates at high gas pressure. Amenable to gas flow cooling/deionization which enhances higher pulse frequency operation and turn-off capability.
High Vacuum Tetrode	3000 V	Grid Voltage	7880	Requires 10 Tubes in Parallel, @ 75.6 cm Long & 30.5 cm Dia.	Water cooled, Eimac $\times$ 2062J, screen grid-2000 V, filament power per tube 6.5 kW, warm up time 30 seconds. (Special tube design can reduce filament power to 2 kW per tube.) Proven performance with tubes commercially available.
Crossed-Field Switch (X-field switch)	500-1000 V	Magnetic Field (5000 Ampere turns with fast rise and fall time)	Not Specifically Determined	500 cm^2	Operates at low gas pressure, typically less than 50 milli-torr. Because of sensitivity to gas pressure, heat buildup may limit X-field switch to relatively few on-off cycles of operation at a time. Experimental devices only.
Transistor Array	470 V	Base Current	3700	Large Assembly	Array of 2676 (223 $\times$ 12) W D60T transistors with associated protective diodes and high voltage isolated transistor base drive circuitry. Transistors are commercially available, however such a large high voltage array has not been assembled and may be impractical.

86-0120-34

63

parameter values shown in table 3 for methane. The control power gain was calculated using equation (32) and the assumptions stated in section 2.4.

For the high-vacuum tube approach, a vacuum tetrode was chosen over a triode because of the higher control gain it offered. The control power was the required input power to the control grid. Ten tubes in parallel would be required to carry the total current. The total filament power is 65 kW; however, tubes with special cathode design could reduce it to 20 kW.

The crossed-field switch[48,49,50,51,52] has been studied for a number of years. It operates in the low-pressure end of the Pashen Curve (i.e., on the order of 50 milli-torr) where the breakdown voltage varies radically with very small changes in pressure. This situation presents the possibility that discharge heat in a relatively few pulses could drastically alter the parameters of the crossed-field switch away from the desire operating region. Fast magnetic field rise and fall times are required to turn on and turn off the X-field switch. Typically 5000 ampere-turns was required to reach the internal field necessary for ignition due to eddy currents in the vacuum envelope and the electrodes. The power required for the magnetic control field was not cited in the references. Thus, no specific control gain value is shown in table 6; however, use of ignitrons in the control circuit suggest that substantial power is probably expended.

The transistor array for high voltage and cur. it requires the series-parallel operation of many transistors in conjunction with clamping diodes and other components to provide suitable isolation and distribution of transistor base drive. An array structure considered utilized 2676 high-power transistor (WD6OT) assembled in a series/parallel array in a structure insulated for 100 kV. At $110 a transistor, $294,360 would be invested in transistors alone, not counting the cost of associated components and structural assembly. Arithmetic of this type has stymied the

64

use of large transistor arrays in high current at high-voltage applications. Even though the switch voltage drop and control power gain may be adequate for many applications, such large transistor arrays have not been assembled to date and may be impractical.

Comparison of the information in table 6 indicates that for the 100 kV hold off/1 kA case, the e-beam plasma switch provides the highest control power gain and is competitive in size and conduction voltage drop.

A similar switch comparison for the 30 kV/20 kA case suggests that the high vacuum tetrode and transistor arrays are probably impractical because of the sheer number of individual devices that would be required in parallel or series/parallel to carry the total current and hold off the voltage. The crossed-field switch ostensibly will function as a turn on switch at 20kA; however, the self-magnetic field effects[52] generated by the current flowing may preclude its use as a turn off switch. During conduction, the self-generated field has no deleterious effect. When the control magnetic field is removed, however, the self-generated magetic field is of sufficient magnitude to trap electrons and maintain the discharge. Also since the drift direction is now predominantly axial, the plasma will be forced into a new position with an arc as the likely result.

The e-beam plasma switch scales up to the 20kA size linearly using the same plasma discharge relationships as for the lower current switch size. Table 7 shows a range of parameters for an 30 kV holdoff voltage/20kA on-current e-beam plasma switch in methane (CH_4) with gas density $N = 1.08 \times 10^{20}$, discharge gap $d = 1.33$ cm and thin-film field emission electron-beam source.

From the comparison of the various switch types with turnon and turnoff capability at 100 kV/1kA and at 30 kV/20kA, a high voltage switch using an externally ionized plasma appears to be a competitive choice over the other switches types at the lower current value and perhaps the only choice at the higher current value.

65

TABLE 7

PARAMETERS OF 30kV/20kA e-Beam
PLASMA SWITCH (CH$_4$ GAS)

Conduction Voltage Drop	E-Beam Current	Control Power Gain	General Size Indication
552 Volts	0.001 A/cm^2	75,000	20,000 cm^2
1133	0.005	75,000	4,000
2330	0.01	75,000	2,000
3000	0.015	75,000	1,333

80-0120-V-35

SECTION III
CONCLUSIONS

1) Inspection of equation (26) shows that the desirable gas properties for an e-beam switch gas are a high dielectric strength, large magnitudes for the electron-drift velocity and the secondary electron production rate by the beam electrons, a small magnitude for the recombination rate coefficient, a large positive exponent in the expression for the electron-drift velocity vs. E/N, equation (17), and a large negative exponent in the expression for the electron recombination rate coefficient vs. E/N, equation (2). Equation (26) can be used to quickly compare candidate switch gases.

2) The results of the numerical studies of steady-state switch operation presented in figures 8 through 19, and the analytical results presented in figure 20 show that the best gas studied is methane, followed in order by the N_2:Ar = 1:9 mixture, nitrogen, and argon.

3) The results of the numerical studies for methane show that the required physical size for currents of 1KA and 20KA is, respectively, 200 cm^2 and 4000 cm^2 for switches which have a current gain of 1000 and a switch efficiency of 95 percent. Higher efficiencies can be obtained by increasing the switch area, see tables 6 and 7.

4) The maximum achievable current gain is a strongly decreasing function of the electron loss rate due to attachment, and the switch voltage is a strongly increasing function of the attachment rate. However a small amount of attachment is essential in order to obtain switch turn-off times in the $1-100\mu s$ range.

5) Switch turnon times $\sim 1\mu s$ are easily obtainable with electron-beam current densities in the $1-10ma/cm^2$ range,

assuming that the circuit inductance is small enough that it does not limit the turnon time.

6) The high control power gain and the relatively low control voltage of the thin-film field emission cathode coupled with a constant potential electron-acceleration section recommends this type of electron gun for turning on the plasma switch.

7) Comparison of the various switch types with turnon/turnoff capability indicated that high voltage switches using externally ionized plasmas have the potential of being developed into devices that are competitive or superior in size and capability with any other approach providing equivalent electrical performance.

SECTION IV
RECOMMENDATIONS

1) An experimental study should be carried out to measure e-beam sustained plasma discharge properties and to compare them with the values calculated using the model presented in this report. Gases to be studied should include CH_4, $N_2:Ar = 1:9$ mixture, N_2 and Ar. Additions of small quantities of strongly electronegative gases to the above gases/gas mixture should also be considered.

2) Development of thin-film field emission cathodes should be undertaken using a 3-inch diameter silicon wafer. Uniform arrays in the order of 500 to 5000 field emission points per square centimeter should be considered. Also performance of these cathodes at ambient gas pressures ranging from 5×10^{-6} to 1×10^{-9} torr should be evaluated.

REFERENCES

1. B.M. Koval'chuk, V.V. Kremnev and G.A. Mesyats, Soviet Physics-Doklady 15, 167 (1970).

2. B.M. Koval'chuk, Yu. D. Korelev, V.V. Kremnev and G.A. Mesyats, Soviet Radio Engineering and Electron Physics 21, No. 7, 112 (1976).

3. R.O. Hunter, Bull. Am. Physics Soc. 20, 255 (1975); Proc. 1st Int'l. Pulsed Power Conf., Lubbock, Texas, Nov. 1976 (IEEE Cat. No. 76 CH 1147-8 REG 5) paper IC8; U.S. Patent 4,063,130 (1977).

4. P.E. Luft, "Description of a Backward Prolongation Program for Computing Transport Coefficients," JILA Info. Ctr. Rpt. No. 14, (Joint Inst. for Lab. Astrophysics, Boulder, Colorado, October 30, 1975).

5. D.H. Douglas-Hamilton, J. Chem. Phys. 58, 4820 (1973).

6. See, for example, J.D. Daugherty in "Principles of Laser Physics", Edited by George Bekefi (Wiley, New York, 1976) Ch. 9.

7. L. Pages, E. Bertel, H. Joffre and L. Sklaventis, "Energy Loss, Range, and Bremsstrahlung Yield for 10KeV to 100 MeV Electrons in Various Elements and Chemical Compounds." Atomic Data 4, 1 (1974).

8. A.G. Engelhardt, A.V. Phelps and G.C. Risk, Phys. Rev. 135, A1566, (1964).

9. D. Levron and A.V. Phelps, Bull. Am. Phys. Soc. 24, 129 (1979).

10. D.C. Cartwright, A. Chutjian, S. Trajmar and W. Williams, Phys. Rev. 16, 1013, 1041 and 1052 (1977).

11. D. Rapp and P. Englander-Golden, J. Chem. Phys. 43, 1464 (1965).

12. See. T.N. Daniel, J. Dutton and F.M. Harris, J. Phys. D 2, 1559 (1969) and references therein.

13. L.S. Frost and A.V. Phelps, Phys. Rev. 136, A1538 (1964).

14. M. Schaper and H. Scheibner, Beit. Plasma Physics $\underline{9}$, 45 (1969).

15. A.A. Kruithof, Physica $\underline{7}$, 519 (1940).

16. C.W. Duncan and I.C. Walker, J. Chem Spc, Faraday Trans II, $\underline{68}$, 1514 (1972).

17. R.B. Brode, Phys. Rev. $\underline{25}$, 636 (1925).

18. See for example H.D. Morgan and J.E. Mentall, J. Chem. Phys. $\underline{60}$, 4734 (1974) and references therein and T.G. Finn, B.L. Carnahan, W.C. Wells and E.C. Zipf, J. Chem. Phys. $\underline{63}$, 1596 (1975) and references therein.

19. H.F. Winters, J. Chem. Phys. $\underline{63}$, 3462 (1975)

20. T.E. Sharp and J.T. Dowell, J. Chem. Phys. $\underline{46}$, 1530 (1967).

21. D. Rapp and P. Englander-Golden, J. Chem. Phys. $\underline{43}$, 1464 (1965).

22. W.H. Long, W.F. Bailey and A. Garscadden, Phys. Rev. $\underline{A13}$, 471 (1976).

23. D.H. Douglas-Hamilton, J. Chem. Phys. $\underline{58}$, 4820 (1973).

24. Y.J. Shiu and M.A. Biondi, Phys. Rev. $\underline{A17}$, 868 (1978).

25. See, for example, J.A. Rees Ed., "Electrical Breakdown in Gases", (Wiley, New York, 1973). Chs 4-7.

26. T.W. Dakin and J. Gerhold, Electra No. 32, 61 (1974) and No. 52, 67 (1977).

27. D.E. Golden and L.H. Fisher, Phys. Rev. $\underline{123}$, 1079 (1961).

28. A.H. Guenther and J.R. Bettis, J. Phys. D. $\underline{11}$, 1577 (1978).

29. L.E. Kline, D.K. Davies, C.L. Chen and P.J. Chantry, J. Appl. Phys. $\underline{50}$, 6789 (1979).

30. W.J. Pollock, Trans. Far. Soc. $\underline{64}$, 2919 (1968).

31. C.S. Lakshminarasimha and J. Lucas, J. Phys. D. $\underline{10}$, 313 (1977).

32. L.W. Cochran and D.W. Forester, Phys. Rev. $\underline{126}$, 1785 (1962).

33. W. Franke, Z. Phys. $\underline{158}$, 96 (1960).

34. H. Schlumbohm, Z. Phys. $\underline{182}$, 306, 317 (1965).

35. A.H. Cookson, B.W. Ward and T.J. Lewis, Brit. J. Appl. Phys. 17, 891 (1966).

36. J.W. McGowan (private communication).

37. H. Tholl, Z. Phys. 172, 536 (1963).

38. A.E.D. Heylen and T.J. Lewis, Brit. J. Appl. 7, 411 (1956).

39. R.R. Suhre & J.T. Verdeyne, J. Appl. Phys. 47, 4484 (1976).

40. W.M. Hughes, Appl. Phys. Lett. 24, 480 (1974).

41. J.R. Murray & C.K. Rhodes, J. Appl. Phys. 47, 5041 (1976), Section V.

42. J.I. Levatter & S.C. Lin, 31st Gaseous Electronics Conference, Buffalo, N.Y. 1978.

43. S. Sumida et. al. Applied Phys. Lett. 33, 913 (1978).

44. Yu. P. Raizer, "Laser-Induced Discharge Phenomena", (Consultants Bureau, N.Y. 1977).

45. W.M. Clark and G.S. Dunning, Final Report, Contract No. - N00014-72-C-0496, Hughes Research Laboratories, December 1976.

46. C.A. Spindt, I. Brodie, L. Humphrey & E.R. Westerberg, J. Appl. Phys. 47, 5248 (1976).

47. I. Brodie & C.A. Spindt, Applications of Surface Science 2, 149 (1979).

48. M.A. Lutz and G.A. Hofmann, IEEE Trans. PS-2, 11 (1974).

49. M.A. Lutz, R.J. Harvey and H. Altiny-Mees, IEEE Trans. PS-4, 118 (1976).

50. R. Harvey and M.A. Lutz, IEEE Trans. PS-4, 210 (1976).

51. M.A. Lutz, IEEE Trans. PS-5, 273 (1977).

52. R.J. Harvey, M.A. Lutz and H.E. Gallagher, IEEE Trans. PS-6, 248 (1978).

DAT FILM